This is a repository copy of *Environmental controls, morphodynamic processes, and ecogeomorphic interactions of barchan to parabolic dune transformations*.

White Rose Research Online URL for this paper:
http://eprints.whiterose.ac.uk/106679/

Version: Accepted Version

Accepted Manuscript

Environmental controls, morphodynamic processes, and ecogeomorphic interactions of barchan to parabolic dune transformations

Na Yan, Andreas C.W. Baas

Please cite this article as: Yan, Na, Baas, Andreas C.W., Environmental controls, morphodynamic processes, and ecogeomorphic interactions of barchan to parabolic dune transformations, *Geomorphology* (2016), doi:10.1016/j.geomorph.2016.10.033

Title

Environmental controls, morphodynamic processes, and ecogeomorphic interactions of barchan

to parabolic dune transformations

Authors

Na Yan[1, 2] and Andreas C.W. Baas[3]

[1] Department of Geography, King's College London, UK – na.yan@kcl.ac.uk

[2] School of Earth and Environment, University of Leeds, UK – n.yan@leeds.ac.uk

[3] Department of Geography, King's College London, UK – andreas.baas@kcl.ac.uk

Contact Information

Na Yan

Tel: +44 (0) 20 7848 1054

Email: na.yan@kcl.ac.uk; n.yan@leeds.ac.uk

1

Abstract

The transformation of barchans into parabolic dunes has been observed in various dune systems around the world. Precise details of how environmental controls influence the dune transformation and stabilisation mechanism, however, remain poorly understood. A 'horns-anchoring' mechanism and a 'nebkhas-initiation' mechanism have previously been proposed and selected environmental controls on the transformation have been explored by some modelling efforts, but the morphodynamic processes and eco-geomorphic interactions involved are unclear and comparison between different dune systems is challenging. This study extends a cellular automaton model, informed by empirical data from fieldwork and remote sensing, to fully explore how vegetation characteristics, boundary conditions, and wind regime influence the transformation process and the resulting dune morphologies. A 'dynamic growth function' is introduced for clump-like perennials to differentiate between growing and non-growing seasons and to simulate the development of young plants into mature plants over multiple years. Modelling results show that environmental parameters interact with each other in a complex manner to impact the transformation process. The study finds a fundamental power-law relation between a non-dimensional parameter group, so-called the 'dune stabilising index' (S_*), and the normalised migration distance of the transforming dune, which can be used to reconstruct paleo-environmental conditions and monitor the impacts of changes in climate or land-use on a dune system. Four basic eco-geomorphic interaction zones are identified which bear different functionality in the barchan to parabolic dune transformation. The roles of different environmental controls in changing the eco-geomorphic interaction zones, transforming processes, and resulting dune morphologies are also clarified.

Keywords

1.   Introduction

Vegetation is a first-order control on the shape and activity of sand dunes. Bare-sand barchan dunes, with a slip face and two horns extending downwind, can be stabilised by colonising plants and transformed into parabolic dunes, which typically have a U- or V-shaped lobe with two trailing arms pointing upwind encompassing a deflation basin. The transformation of barchans into parabolic dunes has important implications for land use as vegetated dune fields often carry significant socio-economic activity, and there are growing concerns about potential impacts of climatic changes and needs for judicious land management.

The transformation has been studied in a number of regions, including Råbjerg Mile in Denmark (Anthonsen et al., 1996), the Mediterranean Coast of Israel (Tsoar and Blumberg, 2002; Ardon et al., 2009), Manawatu in New Zealand (Hesp, 2001; Hart et al., 2012), Ceara in Brazil (Duran et al., 2008), the Northern Great Plains in Canada (Wolfe and Hugenholtz, 2009; Barchyn and Hugenholtz, 2012a; Barchyn and Hugenholtz, 2012b), Navajo Country in Arizona (Hack, 1941), Hanford in Washington (Stetler and Gaylord, 1996), and White Sands in New Mexico (McKee, 1966; Reitz et al., 2010). Transformation may be caused by climatic changes favouring vegetation establishment and growth, such as an increase in precipitation or temperature (Stetler and Gaylord, 1996; Wolfe and Hugenholtz, 2009), or anthropogenic impacts such as a reduction in grazing activity or the artificial restoration of vegetation (Hesp, 2001; Ardon et al., 2009). Previous work has proposed a 'horns-anchoring' mechanism and a 'nebkhas-initiation' mechanism for the transformation (reviewed and discussed by Yan and Baas, 2015).

The underlying mechanisms and exact eco-geomorphic interactions that drive the transformation are not yet fully determined, partly because of the complex environmental controls, and partly because of the absence of empirical field data over the long time-scales involved. Some progress has been made through an integration of computer modelling with field measurements and remote sensing techniques (Duran et al., 2008; Nield and Baas, 2008b; Barchyn and Hugenholtz, 2012a; Barchyn and Hugenholtz, 2012b), but the impacts of different environmental controls have not yet been explored and comparisons between different dune systems have not been established.

This paper presents simulation results from a cellular automaton model that has been extended from DECAL, the Discrete Eco-geomorphic Aeolian Landscapes model (Nield and Baas, 2008a; Nield and Baas, 2008b; Baas and Nield, 2010), by incorporating seasonality and a dynamic growth function, parameterised by field measurements and remote sensing of a vegetated dune field in Inner Mongolia, China. The Extended-DECAL is used to: 1) explore the role of key environmental factors in a barchan to parabolic dune transformation, 2) develop a non-dimensional 'stabilising index' that can be used to compare transformations across different dune systems, 3) illustrate eco-

3

geomorphic interaction zones involved, and 4) demonstrate how modelling outcomes can assist in paleo-environmental reconstruction and guide judicious land-management decisions.

2.   Regional setting

The North of the Ordos Plateau, Inner Mongolia, China (Fig. 1) comprises a farming-pastoral ecotone, with an arid continental temperate climate in the northwest and a semi-arid monsoonal climate in the southeast (Zheng et al., 2005; Li et al., 2009). The field site is located in the Hobq Desert, between two seasonal rivers, in a transition zone with mobile crescentic dunes in the north, vegetated parabolic dunes in the centre, and sand sheets in the south.

The region experiences a temperate continental climate with cold, dry and windy winters and hot, wet and less windy summers. Meteorological data from Dongsheng station indicate an annual mean temperature of 6 ^{o}C, with the lowest and highest monthly mean temperatures in January (-11 ^{o}C) and July (21 ^{o}C), respectively. Mean annual precipitation is 370 mm, 80 % of which falls in the period between June and September. Sand drift potentials of the wind climate were analysed using the Fryberger method (Fryberger, 1979; Bullard, 1997), with the sand transport threshold wind speed calculated using Bagnold's (1941) equation and the median grain size of 0.27 mm determined from local soil samples collected in a previous study (Yan, 2010). The results show that the area represents a medium-energy wind environment with sand drift potentials varying moderately (Fig. 1c). The annual sand drift potential is 36.63 VU with a RDP/DP of 0.48. The sand drift potential shows a strong seasonal variation, high in Spring and Winter and low in Summer, especially during the period from June to October.

Vegetation in the study region is dominated by Ordos Sagebrush (Artemisia ordosica), a native, deciduous, psammophytic shrub species. Other species include Mongolian Sweetvetch (Hedysarum mongolicum), Sand Rice (Agriophyllum squarrosum), Broom Sweetvetch (Hedysarum scoparium) and Littleleaf Peashrub (Caragana microphylia). Ordos Sagebrush can out-compete other species and occupy a large area exclusively. The height of the Ordos Sagebrush is 0.5 - 1.0 m with maximum canopy coverage of approximately 1.0 m^2 (Yang et al., 2008; Zhang et al., 2008; Li et al., 2010). Their natural propagation is primarily from seed, although occasionally plants can propagate from clonal branches (Wang et al., 2002). Seedlings grow rapidly and endure partial burial as long as it does not reach their terminal buds. Deep roots may enable seedlings to survive some denudation, but severe erosion can cause plants to die of desiccation (Li et al., 2010). The growth of the Ordos Sagebrush has a strong seasonality, germinating and growing its leaves in March, producing shoots in June, and reaching its prime from July to September (Wang et al., 2002). From late October onward, leaves turn yellow and are eventually shed.

Five parabolic dunes with varying mobility at the site were investigated with field surveys of vegetation and topography in July 2011, and three of these were investigated again in September 2012. Plant abundances were

4

recorded in 5×5 m^2 quadrats located strategically on and around each dune, with height, width, and length of individual canopies recorded. Beyond the quadrats the dimensions of 2264 Ordos Sagebrush individuals were also recorded as well as geo-located. Geo-location of survey quadrats and shrub individuals was by RTK-dGPS with horizontal accuracy of 1 cm and vertical accuracy of 2 cm, which was also used for collecting detailed topographic surveys of the dunes for DEM generation (see Fig. 2).

3.   Modelling

The interaction between vegetation and sand transport is dependent on the characteristics of specific plant species (Buckley, 1987; Bendali et al., 1990; Maun, 1998; Gilbert and Ripley, 2010; Yan and Baas, 2015). Annual grasses are short-lived and perish soon after episodic rainfall events, whereas perennials can influence the temporal and spatial patterns of sand transport over many years to influence dune development. Most perennial grasses grow quickly and spread over the ground surface. The overall coverage of the grass assemblage increases surface roughness and reduces sand transport significantly, so that a surface cover of ~15 % is sufficient to stop most sand transport (Wiggs et al., 1995; Lancaster and Baas, 1998). Perennial shrubs and some clump-like grasses, such as Ordos Sagebrush and Marram Grass (Tsoar and Blumberg, 2002), form separate individual roughness elements that modify the wind velocity profile near the surface and create zones of accelerated- and decelerated-airflows as well as landscape connectivity (Ranwell, 1972; Hesp, 1981; Okin et al., 2015).

To simulate in DECAL the growth of perennial clump-like plants such as the Ordos Sagebrush and their age-dependent impact on sand transport we introduce a 'dynamic growth function' in Section 3.1, that includes multi-year growth and also differentiates growing and non-growing seasons. Section 3.2 illustrates how key environmental controls in the model are parameterised based on field measurements and remote sensing imagery analysis. The strategy that was used to explore different roles and sensitivities of environmental parameters in the barchan-to-parabolic dune transformation is presented in Section 3.3.

3.1.   Algorithm and dynamic growth function

The DECAL model (Nield and Baas, 2008b) expanded on Werner's (1995) cellular automaton for simulating bare-sand dunes by incorporating a vegetation component in the form of 'vegetation effectiveness', ρ, to explore vegetated dune landscapes. It represents the capability of vegetation to reduce sand transport, and is loosely conceptualised as a Frontal Area Index or vegetation coverage. The change in vegetation effectiveness ($\Delta\rho$) on a cell is determined by its local sedimentation balance (Δh) via a so-called 'growth function' that reflects the capability of the vegetation species to withstand erosion and sand burial. Vegetation growth/decline (updating of ρ) is effected

only once per modelling year. The range of ρ that can exert impact on sand transport [0, 1] is a subset of its physiological range [$\rho_{\text{physioMin}}$, $\rho_{\text{physioMax}}$]. A negative ρ is analogous to a situation of nutrient depletion, and allows a dormancy period before vegetation germinates again ($\rho > 0$), whilst $\rho > 1$ allows vegetation to grow beyond the density or coverage threshold that stops sand transport.

To simulate the growth of clump-like perennials, the Extended-DECAL adopts some different perspectives. The ρ in a cell now relates to the size or coverage of a single individual shrub, representing an Ordos Sagebrush, and is initialised on bare surfaces with $\rho_{\text{physioMin}}$, where a negative ρ includes situations where the shrub has started to grow (seedlings or a few small stems above ground) but has not yet reached a minimal size large enough to impede sand transport. Furthermore, the local sedimentation balance has an impact on the germination of seeds: the extended algorithm specifies a germination range of near-neutral sedimentation balance within which a shrub can be initiated. Unlike the original DECAL where growth functions apply to all cells uniformly and vegetation is assumed to be viable always and everywhere, in the extended algorithm vegetation growth only occurs on cells where seeds have germinated.

Ordos Sagebrush exhibits seasonal growth, and this is included in the Extended-DECAL by specifying four seasons per year with a vegetation update after each one, and by defining a positive growth rate α (i.e., an increasing impact on sediment transport) for the two growing seasons (April-May-June, July-August-September), together with a negative 'growth' rate β (i.e., a decreasing impact on sand transport) during the non-growing seasons (October-November-December, January-February-March), the latter to represent the shrub shedding its leaves. These parameters define the growth and decline rate at a neutral sedimentation balance ($\Delta h = 0$), as shown in Fig. 3. The other, linear sections of the growth function are defined by the sedimentation balance range (a, b) within which the shrub maintains its ability to grow, and the maximum erosion tolerance (τ_{eroMax}) and maximum deposition tolerance (τ_{depMax}), that define (respectively) negative or positive sedimentation balances beyond which the shrub's impact is entirely removed (e.g. by complete erosion and uprooting, or by complete burial). In the non-growing seasons, the shrub sheds its leaves, reducing its impact on sediment transport, and decreasing ρ at the decline rate of β (for $\Delta h = 0$). Erosion and deposition during the non-growing seasons then further exacerbate the decline down to complete removal at τ_{eroMax} and τ_{depMax}.

While the original DECAL employs a fixed growth function for all vegetation of a given species, regardless of its size or age, the Extended-DECAL introduces a growth/decline relationship with the shrub's size or age: the τ_{eroMax} and τ_{depMax} are not constant, but are determined each season by scaling the existing ρ on a cell, which relates closely to the size or age of the shrub, against two fundamental shrub parameters, the physiological erosion tolerance ($\tau_{\text{E\_physioMax}}$) and deposition tolerance ($\tau_{\text{D\_physioMax}}$) properties, defined as the sedimentation tolerances when the plant

6

is at $\rho_{physioMax}$. The maximum growth and decline rates, α and β, are also made a function of the existing ρ (further explained in section 3.2.1 below), and the a and b parameters are set proportional to the τ_{eroMax} and τ_{depMax} of the local shrub (default is 90%). This dynamic growth function represents the fact that shrubs have different capabilities of growth and response to erosion and deposition at different stages of their life cycle. Compared with small seedlings, mature, larger plants usually have greater resilience to surface changes. Mature Ordos Sagebrush, in particular, can survive sand burial as long as they are not completely submerged by sand, and its extensive root systems help anchor shrubs to the ground, keeping sand in check and resisting wind erosion. Section 3.2.1 details how field measurements were used to parameterise the seasonality and dynamic growth function.

3.2. Parameterisation

3.2.1. Vegetation growth

The spatial resolution of the domain is set at 1×1 m^2 to represent the growth of individual shrubs, as the field surveys revealed that 73% of measured individuals had a canopy cover area of 1 m^2 or less (Fig. 4), and this spatial scale ensures sufficient detail in topography and vegetation patterns. The temporal scale is defined by four seasons per year, with vegetation updating after each. This updating interval is long enough to mask potential time-lags between the response of a shrub to environmental changes, while short enough to minimise the likelihood of extreme erosion and deposition swings within a single period that would make the sedimentation balance at the end of that period unrepresentative.

The natural propagation of the Ordos Sagebrush is dominantly from seed, and the germination range of sedimentation balance is set between 0 and +0.1 m season^{-1}, such that germination cannot occur on eroding surfaces and only under zero or minimal deposition. Like most plant species, the growth of the Ordos Sagebrush is a non-linear process with its age. Initial growth form after germination is mostly vertical without significant canopy development. Later, the shrub develops a more horizontal and outstanding canopy, and vertical development dwindles. The (scalar) canopy size of a plant (V$^{1/3}$, where V is the canopy volume in m^3) may thus be used as a linear proxy for the age of the plant (t_{age}). Meanwhile, ρ in a grid cell is assumed to linearly correlate with canopy cover area. Since the field surveys provided data on all three dimensions for 2264 Ordos Sagebrush individuals (Appendix A), a relationship between ρ and t_{age} can be defined by a linear relationship between ρ and canopy cover area (up to 1 m^2) linked with a linear relationship between t_{age} and canopy size.

The canopy cover of shrubs within a range of [0, 1] m^2 was linearly scaled as ρ over a physiological range of 2 units. A power-law regression of the field survey data established (with R^2 = 0.97) that a canopy cover of 1 m^2 is equivalent to a canopy size of 0.91 m (which reflects age). As it takes about 3 years for the Ordos Sagebrush in the

7

study region to develop a canopy cover of 1 m^2, the size of each shrub in the range of [0, 0.91] m was scaled as shrub age with a range of [0, 3] yr. The growth rate (α) for a shrub at a specific age can then be defined from the derivative of the regression function relating t$_{age}$ and (ρ - $\rho_{physioMin}$), which comes to:

$$\alpha = 0.1915 \left(\frac{\rho - \rho_{physioMin}}{0.1711}\right)^{0.5532} \tag{1}$$

The decline rate of a shrub in a non-growing season (β) is assumed to be simply proportional to its existing ρ:

$$\beta = \eta \left(\rho - \rho_{physioMin}\right) \tag{2}$$

where: η is a decline coefficient of vegetation in the non-growing seasons, -0.2 by default. An Ordos Sagebrush starts to impact sand transport near the end of its first year of growth, when canopy cover amounts to 0.075 m^2, which scales to a relative ρ of 0.15. The physiological range of ρ is accordingly defined as [-0.15, 1.85] in absolute terms.

3.2.2. Initial conditions

The starting landscape in the simulations consists of a bare barchan sitting on top a flat, fully vegetated sand base. The substratum in the study region is relatively thin and lying over hard fluvial deposits comprised of mixed gravel, sand, silt, and clay, and so simulations cover a range of substratum thickness between 0 and 1.5 m, in steps of 0.3 m. The initial barchan is acquired from a separate simulation run over a bare sand surface under unidirectional wind and without vegetation in the domain in order to produce a dune shape that is consistent with the model environment. Simulations cover a range of sizes of the initial barchan, varying in height from 5.2 to 9.2 m in steps of 1 m (Table 1). The model barchan shape satisfies the morphometric relationship between height and width found in field studies of real barchans (Hesp and Hastings, 1998; Sauermann et al., 2000). The initial ρ of the vegetated surface surrounding the barchan is set to $\rho_{physioMax}$ (no transport), whereas ρ on the bare barchan surface is set to $\rho_{physioMin}$, where vegetation does not grow until its germination condition is satisfied.

3.2.3. Sand transport regime

The sand transport regime in the study region was estimated by combining satellite image interpretations and field measurements. Three Google Earth images from 2005, 2010 and 2012 were geo-rectified and co-registered with a 0.6 m resolution 2007 Quick Bird panchromatic image, subject to an RMS error of 1.14 pixel or 0.68 m. Migration rates over successive periods for a representative dune lobe were determined with the method of Levin and Ben-Dor (2004), detailed in Appendix B, yielding an average migration rate, R, of approximately 5 m yr^{-1}.

Volumetric sand transport rate [q_v, m^3 m^{-1} yr^{-1}] over a longitudinal cross-section of a dune can be determined from its migration rate as: $q_v = \overline{H}R$, where $\overline{H}$ is the average height of the section [m], as long as there is no external sand input and topographic profile changes are minimal. Highest transport rates occur over the crest of a parabolic dune lobe, and so maximum volumetric flux at the study site was derived as the product of the lobe migration rate and the height of the crest. The latter was determined from the topographic field surveys as 4 m, yielding a maximum q_v of 20 m^3 m^{-1} yr^{-1}, which was then assumed to represent the sand transport potential at the study site for model parameterisation. A sand transport rate of 20 m^3 m^{-1} yr^{-1} is comparable to that of many other parabolic dune fields, such as Santa Catarina Island in Brazil (Bigarella et al., 2005), Anglesey in the United Kingdom (Ranwell, 1958; Bailey and Bristow, 2004), and Bigstick Sand Hills and Great Sand Hills in Canada (Wolfe and Lemmen, 1999; Hugenholtz et al., 2008).

The potential sand transport rate in the DECAL algorithm is defined as: $q = h_s l / (p_d I)$, where h_s is the slab height [m], l is the transport length [m], p_d is the slab deposition probability over bare sand, and I is the time-scale that one iteration represents [yr]. In the simulations here the slab height is set to one tenth of the spatial resolution (0.1 m) to provide sufficient vertical resolution on burial and erosion, and which is also close to the minimum thickness suggested by Nield and Baas (2008b). Deposition probability is set to 0.6 and transport length as 1 cell (1 m), commensurate with the default values of previous DECAL studies. As suggested in Nield and Baas (2008b) the potential sand transport rate is then determined by the definition of the time-scale I, the modelling time that one iteration represents. Given the other parameter settings the iteration I is subsequently defined as $1/120^{th}$ of a year (i.e. 120 iterations per year) to yield a modelled potential transport rate of 20 m^3 m^{-1} yr^{-1}. Although the sand rose of Fig. 1c displays variable transport directions in the region, the satellite imagery indicate parabolic dunes and barchans overwhelmingly orientated from West to East and so the simulated transport is simplified to a unidirectional regime. Seasonal variability in transport rate magnitudes is achieved by allocating varying fractions of the 120 yearly iterations to each of the four seasons (section 3.1) proportional with the distribution of the seasonal RDP percentages to its yearly total, as listed in Table 2.

3.3. Simulation strategy

Four batches of simulations, totalling 1775 scenarios, explore the impacts of five environmental parameters on the transformation of a barchan to a parabolic dune, as shown in Fig. 5. The first batch aims at understanding how changes in the two fundamental vegetation properties, erosion tolerance ($\tau_{E\_physioMax}$) and deposition tolerance ($\tau_{D\_physioMax}$), lead to the development of different dune morphologies and the associated physical processes involved. The second batch explores how the height of the initial barchan (H_0) contributes to the transformation. The third

batch examines how the substratum thickness (D_0) interacts with the other three parameters. The final batch explores different sand transport rates (q) with an attempt to fully examine interactions between all the above parameters and analyse their contributions. Although the results and analysis that follow are based on singular instances for each of the 1775 simulated scenarios, every simulation was repeated at least twice, and the replicates confirmed very similar dune morphologies and outcomes.

4.   Results

We have explored phase diagrams and sensitivity analyses for a number of state variables. First, dune transformations are classified into eight categories in Section 4.1. Then, Section 4.2 describes a typical barchan to parabolic dune transformation, followed by highlights of modelling outcomes in Sections 4.3-4.4. A fully detailed and extensive list of the sensitivity analysis of environmental parameters is provided in Appendix C.

The top of the sandy substratum is referred to as the zero-plane. The fully vegetated area surrounding a dune is referred to as the surrounding plain, whereas the eroded area between trailing arms of a parabolic dune is referred to as the deflation plain. The typical morphology of a parabolic dune is shown in Fig. 6. The normalised dune length (L') is the ratio of dune length (L) to average dune width ($\overline{W}$) during a barchan-to-parabolic dune transformation, reflecting the degree of elongation. The transition time (t_{tran}) is the time when the initial barchan is completely transformed into an active parabolic dune: defined as when the toe of the original barchanoid lobe disappears completely and the inner boundary of the windward slope exhibits a smooth parabolic-shaped curve (the detection algorithm is described in Appendix E). The stabilisation time (t_{stab}) is the time when the resulting parabolic dune has become fully stabilised and covered completely by vegetation at $\rho_{physioMax}$.

4.1.   Classification of resulting dune morphologies

The simulated dunes that develop from an initial barchan surrounded by well-vegetated shrub lands under a unidirectional wind regime can be classified into three primary categories: parabolic, barchanoid, and barchanoid-parabolic dunes, based on the morphology and the plan shape of their lobes (Fig. 7a). The parabolic dunes are further subdivided into four sub-types reported in literature: chevron parabolic, lunate parabolic, typical parabolic, and elongated parabolic dunes, based on whether or not trailing ridges or arms are present and the magnitude of dune elongation. Fig. 7b shows examples of the eight types of resulting dunes. The key difference between chevron and lunate parabolic dunes is the migration form of their dune lobe. Chevron parabolic dunes migrate forward without changing form of their v-shaped lobes. Examples might be found in the parabolic dunefields along the Jafurah Desert in Saudi Arabia (Anton and Vincent, 1986) and in the Navajo County of Arizona (Stetler and Gaylord, 1996). In

10

contrast, the lobes of lunate parabolic dunes exhibit a more rounded crescentic shape with very short arms and change in shape quickly. Lunate parabolic dunes therefore only develop once arms start to appear, similar to some parabolic dunes on the Canadian Prairies (Wolfe and Hugenholtz, 2009), at White Sands of New Mexico (McKee, 1966), and in the Horqin Desert of China (Yan, 2010). Typical parabolic dunes have well-defined trailing arms, with *L'* between 1 and 3. Elongated parabolic dunes, often referred to as hairpin-shaped or long-walled, have trailing arms with *L'* larger than 3, consistent with the definition by Pye (1982). Elongated parabolic dunes in the model show a typical hairpin shape resembling those of the east coasts of Australia (Pye, 1983a; Pye, 1983b; Pye, 1984; Levin, 2011). The barchanoid-parabolic transitional and transverse dunes are intermediate stages between the barchan and the parabolic shapes, whose lobes present a batwing shape in a plan view: a crescentic-shaped windward toe and parabolic-shaped dune edges.

4.2. Vegetation characteristics

Fig. 8 shows a typical barchan-to-parabolic dune transformation. It shows how vegetation first encroaches on its flanks slowing down the migration rate of the horns, whereas the central barchanoid lobe continues to move forward at a high rate. The position or height on the lee slope where vegetation can reach is of particular importance in the transformation, and the boundaries between the parabolic arms and the barchanoid lobe relate to where the vegetation starts to encroach higher up the slip face. As these boundaries migrate toward the centre, the barchanoid lobe (with the toe of the original barchan) disappears and a parabolic dune emerges on completion of the barchan-to-parabolic dune transformation. Vegetation subsequently colonises the windward slope and stabilises the whole dune quickly.

The impact of varying erosion and deposition tolerance on resulting dune morphology is presented in phase diagrams in Fig. 9a & b. These show that a deposition tolerance of less than 3 m season^{-1} prevents vegetation encroachment and stabilisation of the migrating barchan and the dune remains bare and mobile. Beyond this (the upper half of the phase diagrams) it is seen that erosion tolerance is the main control on the formation of trailing arms, with a larger tolerance (i.e. a more negative $\tau_{E\_physioMax}$) leading to longer arms. The presence of chevron dunes at the transition time suggests that the formation of trailing arms is not a prerequisite for the barchan-to-parabolic dune transformation. The phase diagrams furthermore indicate that for a number of scenarios the trailing arms become significantly extended between the transition time and the eventual stabilisation, as shown by changes in classification from t_{tran} to t_{stab} (e.g. from Pr2 to Pr3). The time it takes for the transformed dune to fully stabilise is presented in Fig. 9c (showing only scenarios of the upper half of the phase diagrams), showing that t_{stab} decreases

11

exponentially as deposition tolerance increases. At relatively low deposition tolerance the erosion tolerance has a significant additional control yielding longer stabilisation times for vegetation with greater erosion tolerance. At high deposition tolerance this effect disappears.

For a better insight into the transformations and the impact of the vegetation characteristics it is useful to consider the temporal dynamics of migration rate (Fig. 10) and sand volume of the migrating lobe (Fig. 11) in tandem. Migration rate is higher at a low deposition tolerance but, counter-intuitively, also higher at a greater erosion tolerance (Fig. 10a). The two vegetation characteristics influence the migration rate at different stages however: (i) a higher deposition tolerance slows the dune down almost immediately from the start of a simulation (Fig. 10b), whereas (ii) the erosion tolerance only plays a significant role in the latter part of the transformation, toward the stabilisation (Fig. 10c). Meanwhile, the sand volume of the dune lobe per unit width (V') at t_{stab} is higher at small erosion and small deposition tolerances (Fig. 11a), which is associated with a shorter stabilisation time (cf. Fig. 10c) and a lower dune migration rate (Fig. 10a). This suggests that even though elongated parabolic dunes move downwind a relatively long distance before finally being stabilised, and more sand in the substratum is exposed, eroded, and incorporated into the migrating dunes, there is a more significant sand loss from their lobes to form arms in comparison to parabolic dunes developed under a smaller erosion tolerance. Fig. 11b shows a schematic overview of V' dynamics over the course of the dune transformation, as affected by erosion and deposition tolerance. Deposition tolerance plays a dominant role in determining the general level of V'. As deposition tolerance increases, V' shows a faster initial increase but stabilises earlier, resulting in a smaller final value. Within each group of a given deposition tolerance, a greater erosion tolerance leads to a slower increase in V' and stabilisation at a smaller value. However, the impact of the erosion tolerance on the migration time of a dune before being stabilised is dependent on the magnitude of the deposition tolerance. At low levels of deposition tolerance, the difference in stabilisation time at small erosion tolerance (t_{low}) vs high erosion tolerance (t_{high}) is relatively large, and an increased erosion tolerance extends t_{stab} significantly. Under higher deposition tolerances, the effect of erosion tolerance on stabilisation time is reversed, though the impact stays relatively small. When deposition tolerance is very high, dunes are stabilised quickly regardless of erosion tolerance and the time differences are indiscernible.

Smaller erosion and deposition tolerances generally lead to a later initiation of trailing arms (Fig. 12a), but the 'arms-elongating' duration shortens afterwards and dunes are stabilised more quickly (Fig. 12b). The average arms-elongating rate (v_r) generally increases at a lower deposition and a higher erosion tolerance (Fig. 12c). At a low erosion tolerance (≤ 2.0 m season^{-1}), L' does not show significant difference and the resulting parabolic dunes exhibit

a strong similarity in shape (Fig. 12d); at a high erosion tolerance (> 2.1 m season^{-1}), the deposition tolerance plays a crucial role in determining v_r and L', although t_{ro} persists from the beginning of a simulation.

The 'arms-developing angle' (θ_{arms}) is the angle formed between the two trailing arms of a parabolic dune (Fig. 13a). Negative angles indicate laterally expanding dune lobes, whilst positive angles indicate shrinking dune lobes. Fig. 13b & c suggest that θ_{arms} after stabilisation is governed only by deposition tolerance and is largely independent of erosion tolerance. Kruskal-Wallis testing (Kruskal and Wallis, 1952; Field, 2013) indicates significant differences (p < 0.001) between groups of scenarios with the same deposition tolerance but varying erosion tolerances. With higher deposition tolerance, θ_{arms} increases significantly, i.e., indicating dunes that have shrunk more and more. At lower deposition tolerance, θ_{arms} becomes smaller and the arms run more parallel, which is associated with the formation of more elongated parabolic dunes. When deposition tolerance decreases to 3.0 m season^{-1}, the trailing arms broaden outwards to form a negative angle and a laterally expanding lobe. A negative θ_{arms} is, however, less common because the initial barchan has high mobility and can maintain its crescentic shape and migrate forward over a very long distance before eventually (and relatively quickly) being transformed into a parabolic dune.

4.3. Boundary conditions and sand transport potential

The resulting parabolic dunes at t_{stab} become less elongated as H_0 increases (Fig. 14). The elongated trailing arms developed under higher erosion and lower deposition tolerances appear compromised by a larger H_0. As H_0 increases, a barchan-to-parabolic transformation becomes much less sensitive to a change in erosion or deposition tolerance of vegetation. A smaller initial barchan gains more sand from its sandy substratum and increases in height more significantly than a larger initial barchan. The influence of D_0 also varies considerably on H_0 and the deposition tolerance of vegetation (Fig. 15). It is likely that there is a trade-off between the advantages deriving from a thicker substratum that provides more local sand and the disadvantages resulting from a decrease in the dune migration rate and the associated limitation imposed to shorten its travel distance.

An increase in q generally promotes the development of more elongated parabolic dunes, as examples shown in Fig. 16. A higher erosion tolerance increases L' significantly when q is relatively large but exerts a minimal impact when q is very small, whereas the impact of the deposition tolerance is relatively uniform regardless of the magnitude of q. A smaller H_0 or a thinner D_0 is more sensitive to a change in q. Meanwhile, the dune volume increases progressively with an increase of q, as examples shown in Fig. 17. A high erosion tolerance or a low

deposition tolerance increases the dune volume more significantly at a higher q. The fact that a larger H_0 increases the dune volume to a smaller degree indicates that its substratum provides less sand in comparison to a smaller H_0. A dune on a thinner substratum also incorporates more sand, suggesting that the dune migration rate plays a more significant role in the growth of the dune lobe.

5.   Discussion

Environmental parameters in a dune system interact with each other, determining the processes of the dune transformation and the morphology of the resulting parabolic dunes in a complex manner. Dimensional analysis and non-dimensionalisation, Buckingham's Π-theorem for example, have been widely used in extracting the fundamental physical processes governed by key parameters. The role of each parameter and their interactions can be easily identified because a non-dimensional number is independent of the magnitudes of the base units involved. The same phenomenon hence can be compared across different systems. In Section 5.1, we present a fundamental relation between environmental controls expressed by a non-dimensional number termed the 'dune stabilising index', and the plan-view morphology of the resulting parabolic dunes expressed by a 'normalised migration distance', a relation that controls a barchan-to-parabolic dune transformation. Examples are also provided to show how the non-dimensional relation can aid understanding of past and future barchan-to-parabolic dune transformations. Section 5.2 elucidates the fundamental physical mechanism, followed by a detailed discussion on four basic ecogeomorphic interaction zones in Section 5.3. Finally, Section 5.4 discusses the applicability of the Extended-DECAL.

5.1.   Non-dimensionalisation

Dimensional analysis combined with the trends and relations that have been observed in the modelling results suggest a non-dimensional dune stabilising index [S_*], defined by the environmental parameters and the stabilising time [t, yr], elapsed since the start of the transformation, as:

$$S_* = -\frac{\tau_{E\_physioMax}{}^q}{H_0 D_0 \tau_{D\_physioMax}} t \tag{3}$$

Plotting the normalised migration distance ($M/\overline{W}$, where M is the migration distance of the dune crest, [m]) as a function of the dune stabilising index shows a strong power-law relationship (with R^2 of 0.90), as shown in Fig. 18a:

$$M/\overline{W} = 0.07 \, S_*{}^{0.64} \tag{4}$$

14

The competence of the index is illustrated in Fig. 18b. It shows a sample of dunes at various stages of transformation under a variety of environmental parameters (listed in Table 3), but all with identical $S_* = 400$. The ratio of their migration distance to average width is highly consistent (see $M/\overline{W}$ in Table 3).

The power-law relationship may be used to estimate the time that has elapsed since the start of a barchan-to-parabolic transformation. Fig. 19 shows DEMs of two semi-mobile parabolic dunes in the study region (D1 and D2 in Fig. 1) that have been transforming from barchan dunes, with the toes of the initial barchans indicated by the broken relics of vegetated hummocks (back-ridges) upwind. A pit dug during the field campaign indicated a sandy substratum thickness of ~0.6 m. Assuming that the height of each original barchan is similar to the height of the current parabolic dune (crest height relative to the bottom of the slip face), measuring the migration distances and average widths from the DEM, and using the standard sand transport rate of 20 m^3 m^{-1} yr, Equations 3 and 4 can be solved to yield the time elapsed since the start of the transformations: 47 years in both cases (see Table 4 for details). Although it is difficult to evaluate the accuracy of these hindcasts due to the absence of long-term historic remote sensing imagery, they represent a plausible time-scale and this stabilisation might result from widespread desertification-combatting and afforestation activities that were implemented around 1980 in this region. If repeated topographic measurements are available, a discretised derivative of Equation 3 provides a simpler approach to an estimation of t without need to resolve explicitly the environmental parameters:

$$t = \Delta t \left[\left(\frac{\overline{W_1}}{\overline{W_2}} \frac{L_2}{L_1} \right)^{1/0.64} - 1 \right]^{-1} + \Delta t \qquad (5)$$

where: Δt is the time interval between the two observations at t_1 and t_2. This method does require a temporal scale on the order of decades and a steady dune transformation process.

The non-dimensional dune stabilising index proposed above is somewhat similar to the dimensionless fixation index, θ, proposed by Duran and Herrmann (2006) and also reported by Reitz et al. (2010), which involves the initial barchan volume (V), sand flux (Q), and vegetation growth rate (V$_v$). Their simulations suggest that barchans transform into parabolic dunes when $\theta < 0.5$. The scenarios are quite different, however, since their dunes develop over non-erodible surfaces, and interact with grassy vegetation, whereas our modelling efforts simulate dune transformations on an erodible bed, and interacting with large shrubs. It is further difficult to compare θ with our results here because V$_v$ represents an explicit vertical growth rate of plants, which is different from the vegetation effectiveness used in DECAL. Erosion and deposition in Duran and Herrmann model is furthermore treated as undifferentiated absolute surface change, whereas vegetation in DECAL has different capabilities of withstanding erosion and sand burial, and their model does not include seasonality. Nevertheless, θ is qualitatively comparable to

15

S_* in respect of how wind regime, sand availability, and vegetation characteristics influence dune stabilisation and the barchan-to-parabolic dune transformation. Given the same S_*, a higher sand transport rate (q) or a lower sand availability (H_0D_0) requires a shorter time for an initial barchan to transform into a parabolic dune with the same $M/\overline{W}$ - a system with higher mobility. This is similar to a situation in which a larger Q or a smaller V results in a larger θ. The ratio of the erosion tolerance to the deposition tolerance ($-\tau_{E\_physioMax}/\tau_{D\_physioMax}$) in S_* captures the impact of vegetation on the dune transformation. A decrease in the deposition tolerance, for example, leads to a faster transformation from an initial barchan to a given $M/\overline{W}$ – comparable to the case where a smaller V_v leads to a higher θ.

5.2. Physical processes and mechanisms

The movement of barchan dunes and their interaction with vegetation is a complex balance between local sand burial and deposition tolerance, local erosion and erosion tolerance, and the sequencing of burial and erosion events as the dune passes over a location. As a barchan migrates over a vegetated surface, sand cannot escape from its horns, but is trapped and stabilised by vegetation (Fig. 20). The low amounts of sand in motion near the horns are insufficient to bury and remove vegetation on its lee (controlled by vegetation deposition tolerance), but will decrease vegetation vitality and increase the local surface erodibility when vegetation finds itself on the windward side. Under comparable horn-migration and sand budget scenarios, plants with a higher deposition tolerance can endure more severe subsequent erosion, encouraged by a higher erosion tolerance, facilitating sand-trapping process and the development of trailing ridges or arms (e.g., arms-initiation time and the height of trailing arms). The loss of sand from the lobe to its arms further accelerates dune migration and encourages the development of elongated dune morphology.

As sand availability increases from the horns towards the middle of a lobe, vegetation can no longer survive the significant sand burial at the bottom of the lee slope, and the barchanoid-shaped middle lobe, where the width of the erosion front (W_{ero}) and the width of the deposition front (W_{dep}) are similar in magnitude, moves forward at a relatively constant rate (Fig. 21a). On the parabolic-shaped sections linking the arms with barchanoid lobe, the deposition front is much wider than the erosion front due to lateral avalanching of deposited sand, which disperses the sand sideways, decreases the forward migration rate and encourages vegetation encroachment on the lobe from both sides. A lower deposition tolerance, given the same W_{ero}, enables the front edge of a lobe to migrate forward faster, but this also results in more sideways sand dispersal and developing trailing arms with a smaller positive (even negative) arms-developing angle (illustrated in Fig. 21b). A wider deflation plane then exposes more sediment

for transport, forms a larger lobe, and decelerates dune migration, which can lead to a quicker transformation into a parabolic dune as soon as arms or ridges are initiated.

The significant role of vegetation deposition tolerance in controlling the transformation has been observed in field studies (Hack, 1941; McKee, 1966; Tsoar and Blumberg, 2002; Hansen et al., 2006) and modelling explorations (Duran and Herrmann, 2006; Duran et al., 2008; Barchyn and Hugenholtz, 2012a; Barchyn and Hugenholtz, 2012b). This study confirms that a slight increase in the deposition tolerance can significantly accelerate dune stabilisation and develop less elongated parabolic dune. Although it takes longer time to manifest (when deposition tolerance is relative low), the influence of erosion tolerance is significant in developing long-walled parabolic dunes.

For isolated dunes fully surrounded by a well-vegetated surface, sand supply to the dune body is solely from the sandy substratum. A higher initial barchan dune or a thicker sandy substratum thickness provides relatively abundant sand, encourages the development of trailing arms, and forms a larger arms-developing angle (Fig. 21c). Wiggs et al. (1995) found that partially vegetated dunes of the Kalahari exhibit morphological changes in a similar degree as those of much larger bare dunes in the nearby Namib Desert, and reinforces the fact that the dune migration rate is a function of the dune size (Bagnold, 1941). Barchyn and Hugenholtz (2013) show that depth-limited blowouts migrate and elongate at a high rate and it is more difficult for plants to take root and stabilise their mobile lobes. There are several physical processes restraining one another. A smaller dune migrates at a higher rate, which inhibits the stabilisation by vegetation. A higher migration rate, however, can expose and incorporate more sand from the substratum on its way, thereby decelerating the dune and encouraging the stabilisation process. Sand loss by forming trailing arms may also accelerate dune migration substantially. These processes are significantly influenced by the characteristics of vegetation. As the deposition tolerance decreases, the importance of initial dune size becomes progressively overtaken by the sandy substratum thickness, and the erosion tolerance plays an increasingly significant role. Conversely, as the height of the initial barchan increases, the characteristics of vegetation become less important (Fig. 14).

Sand transport potential determines the capability of wind to transport sand (Nield and Baas, 2008b). A high sand transport rate may severely prevent trailing arms from developing or form a smaller positive or larger negative arms-developing angle (Fig. 21d). As the sand transport potential increases, the transformation generally has a greater sensitivity to all other parameters, in particular, the erosion tolerance and sandy substratum thickness, both of which play a more important role when a dune is more active and maintains its mobility for a longer time. This

indicates that dune mobility may have a great spatial heterogeneity in a vegetated area under a relatively high energy wind regime.

5.3. Ecogeomorphic interaction zones

Two potential mechanisms of the barchan-to-parabolic dune transformation have been proposed by previous studies: 'horns-anchoring' and 'nebkhas-initiation' mechanisms. Our modelling results show that the 'horns-anchoring' mechanism is likely to control the transformation in the study region, and that such transformation involves complicated eco-geomorphic interactions and morpho-dynamics, as an example illustrated in Figs. 22 and 23. Four basic eco-geomorphic interaction zones that bear different functionality in the transformation can be identified going from the outer edge to the dune centre-line:

Zone I: from outer edge to point a. On the edge of the migrating lobe, vegetation experiences minimal sand burial and slight decline. As the deposition rate decreases over time ($\Delta H/\Delta t$ in Fig. 23a), vegetation starts to recover and quickly reaches its optimal state while constantly trapping sand. Vegetation in this zone maintains a high vitality; no erosion occurs. Going from the interacting edge toward the inner boundary of this zone (Point a), sand availability increases slightly and eventually point a forms the crest point of this arm. This zone then develops the outside slope of the parabolic arm.

Zone II: from a to b. As sand availability increases, vegetation undergoes more severe sand burial and decline. Similar to Zone I, vegetation recovers as the deposition rate decreases over time. More significant decline caused by sand burial, meanwhile, enables more subsequent erosion when no more sand is available for further trapping. Although the remobilisation of trapped sand decreases the local height after the passage of the main lobe, recovery of vegetation there is still quick enough to partially preserve the deposited sand. This zone then becomes the inner slope of the trailing arm. Point b eventually becomes the inner boundary of the parabolic arm or the edge of the deflation plain. Zone I and Zone II together comprise the transverse section of the arm.

Zone III: from b to c. Point c is the boundary between the crescentic-shaped central lobe and the parabolic-shaped wing. The temporal change in topography across this section is uniform, but slip face sand deposition increases from b to c, inducing a lateral gradient of the maximum height where vegetation can survive. All vegetation here is eliminated by sand burial during passage of the lobe, and only starts to revitalise again once it finds itself on the deflation plain where sedimentation balance is neutral.

18

Zone IV: from c to d (centre-line). This zone maintains the crescentic shape of the original barchan dune and is highly mobile. The changes in both topography and vegetation are uniform in this zone. In contrast to Zone III where the height of vegetation survival on the slip face gradually decreases from the outside boundary (Point b) towards the inside boundary (Point c), vegetation in Zone IV survives up to a limited and constant height on the slip-face.

The deposition tolerance of vegetation influences the eco-geomorphic interactions in all four zones and the lateral expansion or shrinking of each zone relative to one another as the dune migrates and transforms itself. This significant role in controlling the transformation is in agreement with the findings of Barchyn and Hugenholtz (2012b). The erosion tolerance, meanwhile, influences the formation and boundary of trailing arms in Zone I and II. The gradient in maximum survival height of vegetation on the slip-face in Zone III, meanwhile, defines the degree of deceleration of the parabolic-shaped wing, which slows down the crescentic body in the centre and leads to its transformation into a parabolic shape; an example of this process is shown in Fig. 24a. Because of the deceleration caused by Zone III allowing vegetation to maintain its vitality and because of the associated sand loss to the arms by lateral avalanching, sand eventually is inadequate to supress the presence of newly-grown vegetation on the lee slope and starts to deposit and accumulate on the bare surface of the upper lee slope (transition from Zone IV to Zone III) forming a steeper slope as compared with a bare surface (from t_1 to t_2 in Fig. 24b). As the upwind toe of the dune transect stops migrating, vegetation continuously grows up to a higher vertical position, limiting further available sand for erosion. Once the erosion decreases below vegetation erosion tolerance, the whole transect is quickly stabilised (from t_2 to t_3 in Fig. 24b).

The four eco-geomorphic interaction zones show complicated dynamics in the dune transformation. The changes in environmental parameters can influence the relative proportions and locations of the zones and the resulting dune morphologies. Lower vegetation erosion tolerance develops a smaller portion of Zone I and a wider arms-developing angle. This also induces a greater sand loss in Zone II (by erosion) and thinner or no trailing arms of the resulting dune. An increase in the initial dune height or the substratum thickness decelerates the dune migration rate, enables vegetation to withstand burial better in Zone II-III, and encourages a quicker dune transformation. A higher sand transport rate expands Zone IV and narrows Zone II, leading to a longer transition time.

5.4. Model reflections

This study demonstrates how the Extended-DECAL may be parameterised with empirical data to simulate possible dune transformation scenarios under changes in environmental controls. A key improvement is the 'dynamic' growth function that reflects the relationship between vegetation growth and sand transport impact at differing stages of a plant's life cycle. In this study shrub dimension is used as a proxy for age, but more representative results might be achieved if the relationships between vegetation age, morphology, and its influence on sand transport are acquired. The high erosion and deposition tolerances represent extreme amounts and should not be interpreted as real-world equivalents. Nevertheless, the modelling results provide new insights into the complex interactions between environmental controls, and may be applied to many other parabolic dune fields that are dominated by shrubs and clump-like perennial grasses resembling the growth form of the Ordos Sagebrush, such as marram grass (Ammophila) and sand sage (Artemisia filifolia).

The vegetation seasonality that is incorporated in the Extended-DECAL is of particular importance in areas where dunes migrate periodically such as the Ceará and Sãn Franciso River Strand Plain in Brazil (Barbosa and Dominguez, 2004; Duran et al., 2008), the northern Great Plains in Canada (Wolfe and Hugenholtz, 2009; Hugenholtz et al., 2010), Queensland coasts in Australia (Pye, 1983a; Pye, 1984), and White Sands in New Mexico and eastern Colorado of the United States (McKee, 1966; Madole, 1995; Reitz et al., 2010). The region that we have simulated in our study experiences a climate where the windy season is associated with dry, cold conditions and dormant vegetation, and so the results presented here may not be directly applicable to areas where windy seasons coincide with vegetation growing seasons. However, the seasonality mechanism in the Extended-DECAL is also relevant to the formation of remnant vegetation marks, e.g. arcuate vegetated ridges, as barchans migrate forward periodically (de M. Luna et al., 2009; Levin et al., 2009).

The modelling results show that vegetation on the trailing arms is of particular importance in maintaining the parabolic-shaped dune morphology, as reported in field studies (Robertson-Rintoul, 1990; Muckersie and Shepherd, 1995; Livingstone and Warren, 1996; Wolfe and Hugenholtz, 2009). Wide and high arms are associated with a faster transformation from an initial barchan to a parabolic dune. It is likely that the 'arms-anchoring' mechanism controls the barchan-to-parabolic dune transformations in the study region, as discussed in the previous section regarding the four eco-geomorphic zones identified. To what extent the formation of nebkhas can influence the barchan-to-parabolic dune transformation has not yet been explored, but the impact of small nebkhas below the spatial resolution may be assumed to have been automatically incorporated into the modelling processes via the interaction between the vegetation growth and the sedimentation balance. The impact of large nebkhas has not been specifically

simulated, but their influence on sand transport may be comparable with the combined effect of multiple neighbouring plants. The model, nevertheless, represents already the characteristics of more than 70 % of the overall plant population.

This study explores the barchan-to-parabolic dune transformation from one single initial barchan in the domain. It is recognised that the stoss slope of the initial model barchan is significantly steeper than real-world barchans. This unrealistically steep stoss slope of dunes is a fundamental feature of the original Werner model, which was addressed in work by Momiji et al. (2000) by introducing a wind speed-up rule based on absolute height above datum. We decided not to include wind speed-up in the work presented here, however, partly for computation efficiency reasons but mainly because the steepness of the stoss slope is not a significant influence on the stabilisation process as compared with the other parameter controls, and wind speed-up is also not present in the original DECAL model (Nield and Baas, 2008b).

The spatial arrangement of, and interactions between, multiple neighbouring dunes are beyond the scope of the work presented here, but our results may provide effective strategies for vegetation restoration also in this context. For example, simulations show that widening trailing arms can occur when the initial barchan is migrating at a relatively high rate. In a field with multiple barchans, these migrating dunes may thus connect laterally and develop into transverse ridges. This could be the reason why parabolic dunes with negative arms-developing angles are rarely found.

6.   Conclusions

The Extended-DECAL incorporates the changing impact of plants on sand transport as they grow over multiple years, during different seasons and at different ages. The model can be adapted to different aeolian systems with different vegetation communities, and parameterisation can be informed by field measurements and remote sensing. A relatively low computational demand enables extensive exploration of phase space and allows detailed investigation of interactions between a number of parameters, which can then assist in understanding various eco-geomorphic processes of an evolving dune system in a more integrated manner.

The fundamental mechanism controlling the barchan-to-parabolic dune transformation in the study region has been explored in detail. Vegetation characteristics, in particular its capability to withstand wind erosion and sand burial, play a key role in determining the transformation process and rate. A higher deposition tolerance encourages the stabilisation of a barchan, and leads to a faster dune transformation into a parabolic dune with no or relatively

21

short arms – less elongated and more lunate dune morphology. The erosion tolerance plays a less direct role but is essential to control the formation and elongation of trailing arms or ridges. Sand availability in a closed environment is primarily controlled by the size of dunes and the thickness of sandy substratum underneath. A higher sand availability generally decelerates dune migration and hence encourages a faster dune stabilisation and transformation. An increase in potential sand transport rate accelerates the dune migration, thereby prolonging the transition time significantly.

A new non-dimensional 'dune stabilising index' (S_*) captures the combined influence of the system controls on the barchan-to-parabolic dune transformation. A power-law relation between the dune stabilising index and a normalised migration distance provides a plausible approach for extrapolating historical trajectories of transforming dunes, aiding paleo-environmental reconstruction, and predicting dune mobility. This approach can be potentially used in areas where long-term remote sensing records are available, such as Whites Sand in New Mexico and dune fields in the Canadian prairies (Hugenholtz et al., 2010; Reitz et al., 2010). It also provides an indirect method for monitoring climatic impacts on a dune system by detecting deviations from the power-law relation that may indicate recent changes in system controls. The arms-developing angle closely relates to the rate of dune stabilisation, and may be identified and measured in the field to provide a useful linkage between field measurements and modelling simulations.

The details of the dune transformation process can be understood in terms of local sand erosion, transport, and deposition processes impacting on and moderated by local vegetation growth and decline, displaying characteristic behaviours in four distinct eco-geomorphic interaction zones. These zones can be linked to the consequent topographic development during the transformation, and identification of the zones may be used to monitor the stability of a dune system.

Acknowledgements

References

Anthonsen, K.L. et al. 1996. Evolution of a dune from crescentic to parabolic form in response to short-term climatic changes: Rabjerg mile, Skagen Odde, Denmark. Geomorphology. **17**(1-3), pp.63-77.

Anton, D. and Vincent, P. 1986. Parabolic dunes of the Jafurah Desert, Eastern Province, Saudi Arabia. Journal of Arid Environments. **11**(3), pp.187-198.

Ardon, K. et al. 2009. Dynamics of nebkhas superimposed on a parabolic dune and their effect on the dune dynamics. Journal of Arid Environments. **73**(11), pp.1014-1022.

Baas, A.C.W. and Nield, J.M. 2010. Ecogeomorphic state variables and phase-space construction for quantifying the evolution of vegetated aeolian landscapes. Earth Surface Processes and Landforms. pp.717-731.

Bagnold, R.A. 1941. The physics of blown sand and desert dunes. London: Methuen & Co. Ltd.

Bailey, S.D. and Bristow, C.S. 2004. Migration of parabolic dunes at Aberffraw, Anglesey, north Wales. Geomorphology. **59**(1-4), pp.165-174.

Barbosa, L.M. and Dominguez, J.M.L. 2004. Coastal dune fields at the São Francisco River strandplain, northeastern Brazil: morphology and environmental controls. Earth Surface Processes and Landforms. **29**(4), pp.443-456.

Barchyn, T.E. and Hugenholtz, C.H. 2012a. Predicting vegetation-stabilized dune field morphology. Geophysical Research Letters. **39**.

Barchyn, T.E. and Hugenholtz, C.H. 2012b. A process-based hypothesis for the barchan-parabolic transformation and implications for dune activity modelling. Earth Surface Processes and Landforms. **37**(13), pp.1456-1462.

Barchyn, T.E. and Hugenholtz, C.H. 2013. Reactivation of supply-limited dune fields from blowouts: A conceptual framework for state characterization. Geomorphology. **201**(0), pp.172-182.

Bendali, F. et al. 1990. The dynamics of vegetation and sand mobility in arid regions of Tunisia. Kidlington, ROYAUME-UNI: Elsevier.

Bigarella, J.J. et al. 2005. Sub-tropical coastal dunes: Examples from southern Brazil. Journal of Coastal Research. pp.113-137.

Buckley, R. 1987. The effect of sparse vegetation on the transport of dune sand by wind. Nature. **325**(29), pp.426-428.

Bullard, J.E. 1997. A note on the use of the 'Fryberger method' for evaluating potential sand transport by wind. Journal of Sedimentary Research. **67**(3), pp.499-501.

de M. Luna, M.C.M. et al. 2009. Modeling transverse dunes with vegetation. Physica A: Statistical Mechanics and its Applications. **388**(19), pp.4205-4217.

Duran, O. and Herrmann, H.J. 2006. Vegetation against dune mobility. Physical Review Letters. **97**(18), pp.188001/1-4.

Duran, O. et al. 2008. Measurements and numerical simulations of the degree of activity and vegetation cover on parabolic dunes in north-eastern Brazil. Geomorphology. **102**(3-4), pp.460-471.

Field, A. 2013. Discovering Statistics Using IBM SPSS Statistics. London: SAGE Publications Inc.

Fryberger, S.G. 1979. Dune forms and wind regime. In: McKee, E.D. ed. A study of global sand seas. Washington: US Geological Survey Professional Paper, pp.137-169.

Gilbert, M.E. and Ripley, B.S. 2010. Resolving the differences in plant burial responses. Austral Ecology. **35**(1), pp.53-59.

Hack, J.T. 1941. Dunes of the Western Navajo Country. Geographical Review. **31**(2), pp.240-263.

Hansen, E.C. et al. 2006. Growth and Migration of Parabolic Dunes Along the Southeastern Coast of Lake Michigan. Journal of Coastal Research. pp.209-214.

Hart, A.T. et al. 2012. The Impact of Ammophila arenaria Foredune Development on Downwind Aerodynamics and Parabolic Dune Development. Journal of Coastal Research. pp.112-122.

Hesp, P.A. 1981. The formation of shadow dunes. Journal of Sedimentary Petrology. **51**(1), pp.101-112.

Hesp, P.A. 2001. The Manawatu Dunefield: Environmental Change and Human Impacts. New Zealand Geographer. **57**(2), pp.33-40.

Hesp, P.A. and Hastings, K. 1998. Width, height and slope relationships and aerodynamic maintenance of barchans. Geomorphology. **22**(2), pp.193-204.

Hugenholtz, C.H. et al. 2010. Declining sand dune activity in the southern Canadian prairies: Historical context, controls and ecosystem implications. Aeolian Research. **2**(2-3), pp.71-82.

Hugenholtz, C.H. et al. 2008. Effects of sand supply on the morphodynamics and stratigraphy of active parabolic dunes, Bigstick Sand Hills, southwestern Saskatchewan. Canadian Journal of Earth Sciences. **45**(3), pp.321-335.

Kruskal, W.H. and Wallis, W.A. 1952. Use of Ranks in One-Criterion Variance Analysis. Journal of the American Statistical Association. **47**(260), pp.583-621.

Lancaster, N. and Baas, A.C.W. 1998. Influence of vegetation cover on sand transport by wind: Field studies at Owens Lake, California. Earth Surface Processes and Landforms. **23**(1), pp.69-82.

Levin, N. 2011. Climate-driven changes in tropical cyclone intensity shape dune activity on Earth's largest sand island. Geomorphology. **125**(1), pp.239-252.

Levin, N. and Ben-Dor, E. 2004. Monitoring sand dune stabilization along the coastal dunes of Ashdod-Nizanim, Israel, 1945–1999. Journal of Arid Environments. **58**(3), pp.335-355.

Levin, N. et al. 2009. Modelling the formation of residual dune ridges behind barchan dunes in North-east Brazil. Sedimentology. **56**(6), pp.1623-1641.

Li, Q.S. et al. 2009. Response of spatial distribution pattern of Artemisia ordosica population to the precipitation gradient on Ordos Plateau (in Chinese with English abstract). Chinese Journal of Applied Ecology. **20**(9), pp.2105-2110.

Li, S.-L. et al. 2010. Seedlings of the semi-shrub Artemisia ordosica are resistant to moderate wind denudation and sand burial in Mu Us sandland, China. Trees. **24**(3), pp.515-521.

Livingstone, I. and Warren, A. 1996. Aeolian Geomorphology: An Introduction. Harlow: Longman.

Madole, R.F. 1995. Spatial and temporal patterns of late quaternary eolian deposition, Eastern Colorado, U.S.A. Quaternary Science Reviews. **14**(2), pp.155-177.

Maun, M.A. 1998. Adaptations of plants to burial in coastal sand dunes. Canadian Journal of Botany-Revue Canadienne De Botanique. **76**(5), pp.713-738.

McKee, E.D. 1966. Structures of dunes at white sands national monument, New Mexico. Sedimentology. **7**(1), pp.3-69.

Momiji, H. et al. 2000. Simulation of the effect of wind speedup in the formation of transverse dune fields. Earth Surface Processes and Landforms. **25**(8), pp.905-918.

Muckersie, C. and Shepherd, M.J. 1995. Dune phases as time-transgressive phenomena, Manawatu, New Zealand. Quaternary International. **26**, pp.61-67.

Nield, J.M. and Baas, A.C.W. 2008a. The influence of different environmental and climatic conditions on vegetated aeolian dune landscape development and response. Global and Planetary Change. **64**(1–2), pp.76-92.

Nield, J.M. and Baas, A.C.W. 2008b. Investigating parabolic and nebkha dune formation using a cellular automaton modelling approach. Earth Surface Processes and Landforms. **33**(5), pp.724-740.

Okin, G.S. et al. 2015. Connectivity in dryland landscapes: shifting concepts of spatial interactions. Frontiers in Ecology and the Environment. **13**(1), pp.20-27.

Pye, K. 1982. Morphological development of coastal dunes in a humid tropical environment, Cape Bedford and Cape Flattery, North Queensland. Geografiska Annaler Series a-Physical Geography. **64**(3-4), pp.213-227.

Pye, K. 1983a. The coastal dune formations of northern Cape York Peninsula, Queensland. Proceedings of the Royal Society of Queensland. **94**, pp.33-39.

Pye, K. 1983b. Dune formation on the humid tropical sector of the North Queensland Coast, Australia. Earth Surface Processes and Landforms. **8**(4), pp.371-381.

Pye, K. 1984. Models of transgressive coastal dune building episodes and their relationship to Quaternary sea level changes: a discussion with reference to evidence from eastern Australia. In: Clark, M.W. ed. Coastal Research: UK Perspectives. Norwich: Geo Books, pp.81-104.

Ranwell, D. 1958. Movement of vegetated sand dunes at Newborough Warren, Anglesey. Journal of Ecology. **46**(1), pp.83-100.

Ranwell, D. 1972. Ecology of salt marshes and sand dunes. London: Chapman and Hall.

Reitz, M.D. et al. 2010. Barchan-parabolic dune pattern transition from vegetation stability threshold. Geophysical Research Letters. **37**.

Robertson-Rintoul, M.J. 1990. A quantitative analysis of the near-surface wind flow pattern over coastal parabolic dunes. In: Nordstrom, K.F., et al. eds. Coastal Dunes Form And Processes. Chichester: John Wiley & Sons Ltd., pp.57-78.

Sauermann, G. et al. 2000. The shape of the barchan dunes of Southern Morocco. Geomorphology. **36**(1–2), pp.47-62.

Stetler, L.D. and Gaylord, D.R. 1996. Evaluating eolian-climatic interactions using a regional climate model from Hanford, Washington (USA). Geomorphology. **17**(1–3), pp.99-113.

Tsoar, H. and Blumberg, D.G. 2002. Formation of parabolic dunes from barchan and transverse dunes along Israel's Mediterranean coast. Earth Surface Processes and Landforms. **27**(11), pp.1147-1161.

Werner, B.T. 1995. Eolian dunes: Computer simulations and attractor interpretation. Geology. **23**(12), pp.1107-1110.

Wiggs, G.F.S. et al. 1995. Dune mobility and vegetation cover in the Southwest Kalahari desert. Earth Surface Processes and Landforms. **20**(6), pp.515-529.

Wolfe, S.A. and Hugenholtz, C.H. 2009. Barchan dunes stabilized under recent climate warming on the northern Great Plains. Geology. **37**(11), pp.1039-1042.

Wolfe, S.A. and Lemmen, D.S. 1999. Monitoring of dune activity in the Great Sand Hills region, Saskatchewan. In: Lemmen, D.S. and Vance, R.E. eds. Holocene Climate and Environmental Change in the Palliser Triangle: a Geoscientific Context for Evaluating the Impacts of Climate Change on the Southern Canadian Prairies. Geological Survey of Canada Bulletin 534, pp.199-210.

Yan, N. 2010. Surface process and morphological evolution of parabolic dunes. Msc. thesis, Beijing Normal University.

Yan, N. and Baas, A.C.W. 2015. Parabolic dunes and their transformations under environmental and climatic changes: Towards a conceptual framework for understanding and prediction. Global and Planetary Change. **124**(0), pp.123-148.

Yang, H.X. et al. 2008. Comparative study on spatial patterns of Artemisia ordosica populations in the Mu Us sandy land (in Chinese with English abstract). Acta Ecologica Sinica. **28**(5), pp.1901-1910.

Zhang, Z.-S. et al. 2008. Distribution and Seasonal Dynamics of Roots in a Revegetated Stand of Artemisia ordosica Kracsh. in the Tengger Desert (North China). Arid Land Research and Management. **22**(3), pp.195-211.

Zheng, Y. et al. 2005. Vegetation responses along environmental gradients on the Ordos plateau, China. Ecological Research. **21**(3), pp.396-404.

(a)

(b)

(c)
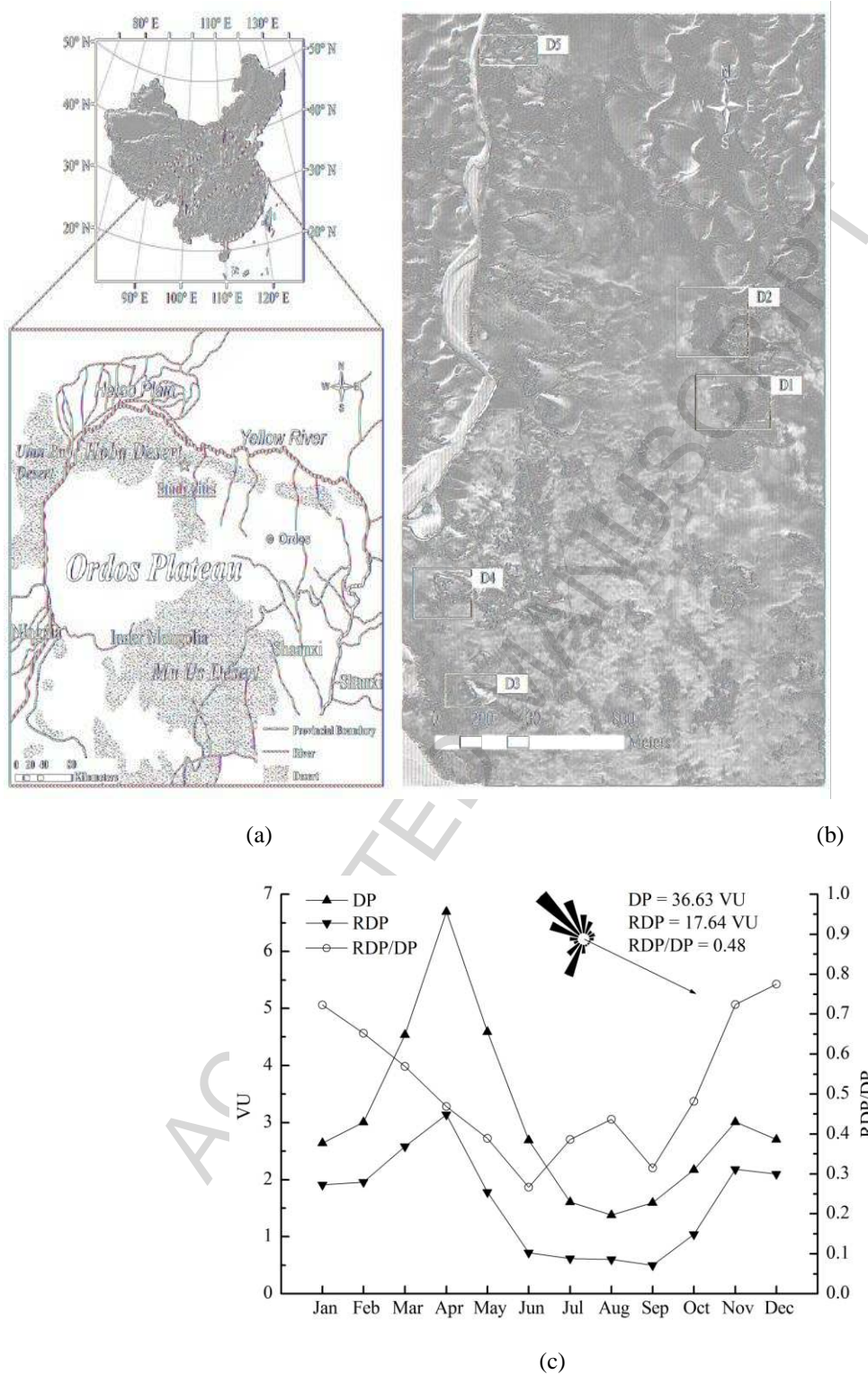
Figure 1. Study region. (a) Location of study sites. (b) Surveyed parabolic dunes, labelled D1 − D5 on a Quick Bird

image in 2007. (c) Sand drift potential in different months.

(a)   (b)
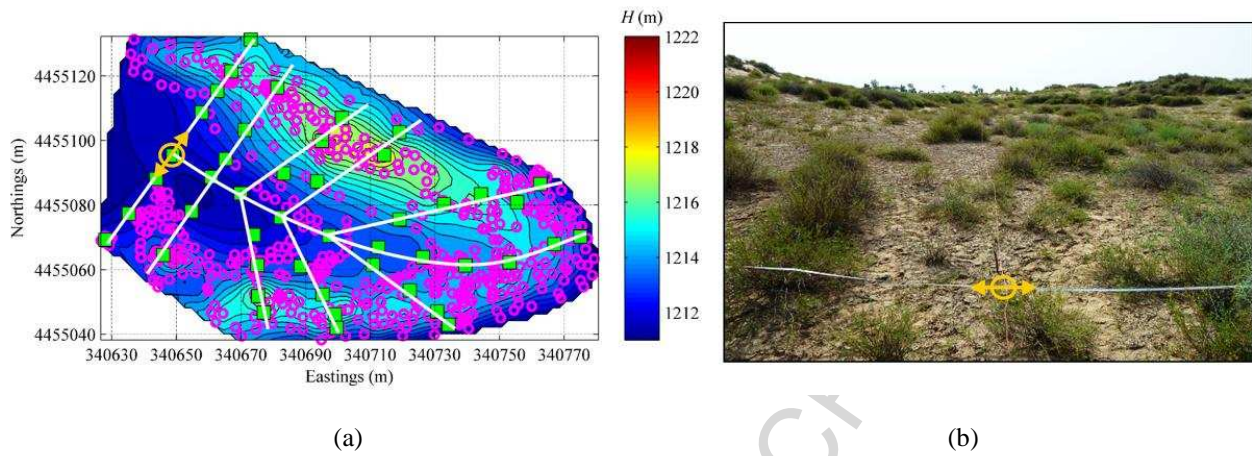
Figure 2. Field survey of a stabilised parabolic dune (D3) at the Ordos Plateau: (a) locations of quadrats (green squares) and measured Ordos Sagebrush individuals (magenta circles), overlain over DEM with 0.4 m contour interval, generated from dGPS survey; and (b) view from the deflation plane, location indicated with orange symbol in (a), looking toward the lobe.
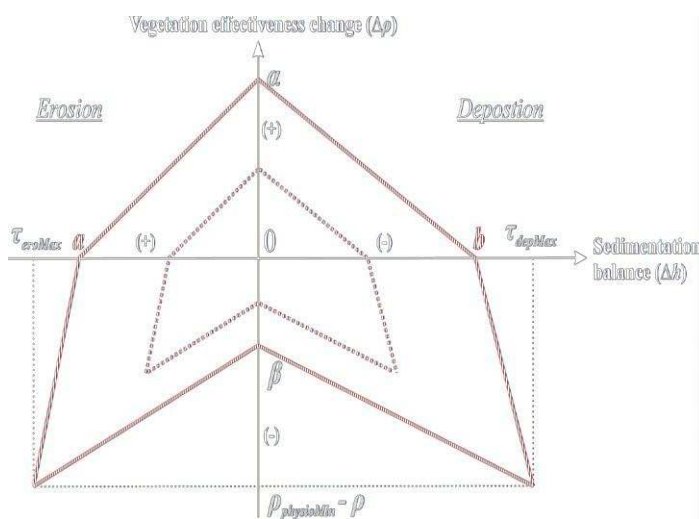
Figure 3. Examples of growth functions in both growing seasons (red lines) and non-growing seasons (blue lines). α and β are the 'growth' rates of vegetation in growing seasons and non-growing seasons respectively. The dotted lines show growth functions for a smaller size of shrub.
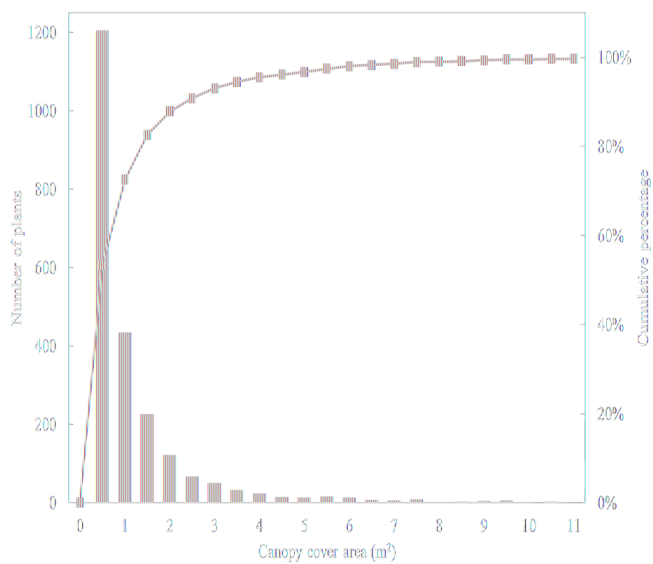
Figure 4. Histogram and cumulative percentage of canopy cover area of Ordos Sagebrush measured in the field.
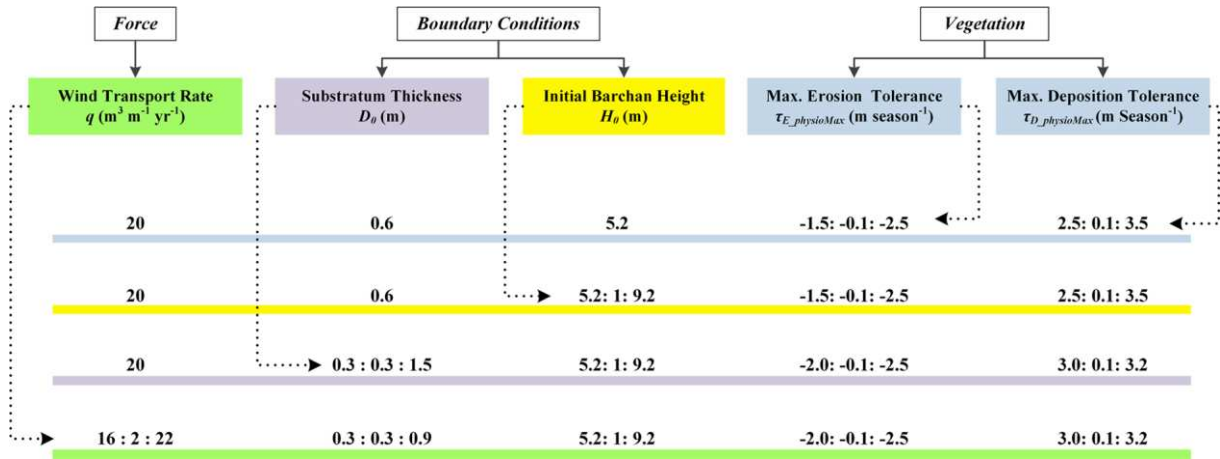
Figure 5. Exploration framework of key environmental parameters with numbers (# : # : #) indicating minimum value : increment step : maximum value of each batch of simulations.

(a)   (b)
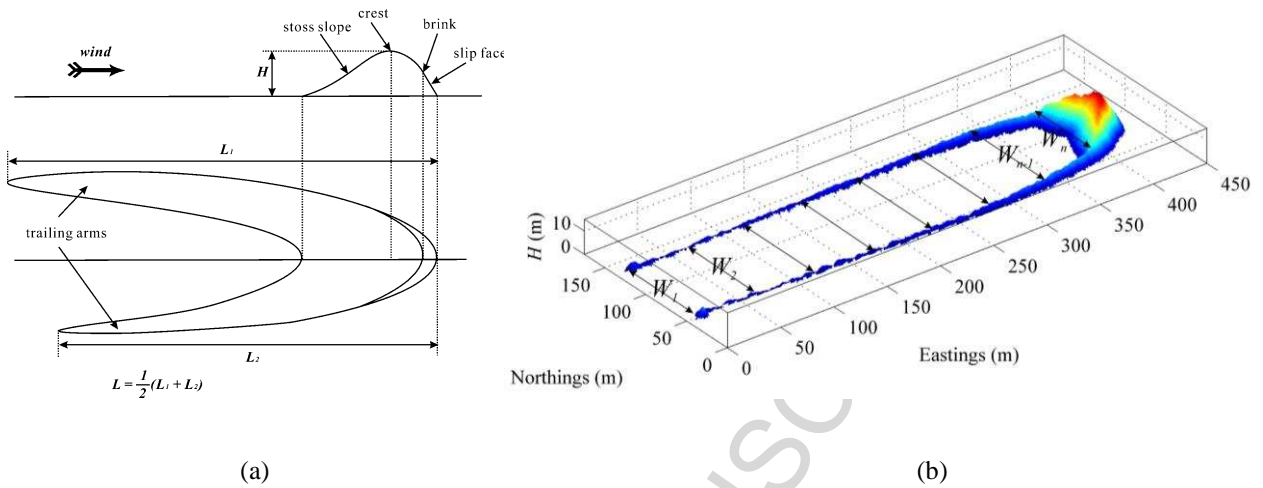
Figure 6. (a) The typical morphology of a parabolic dune. L is the dune length - the average longitudinal distance between the frontal edge of the dune lobe and the tips of the trailing arms. H is the height of the dune crest above the zero-plane. (b). Calculation of the average dune width $\overline{W} = \sum_{i=1}^{n} W_i / n$. The separation between an arm and the lobe (W_n) is defined as where the topography starts to significantly increase beyond the average or trend of the arm crest (the detection algorithm is described in Appendix D).
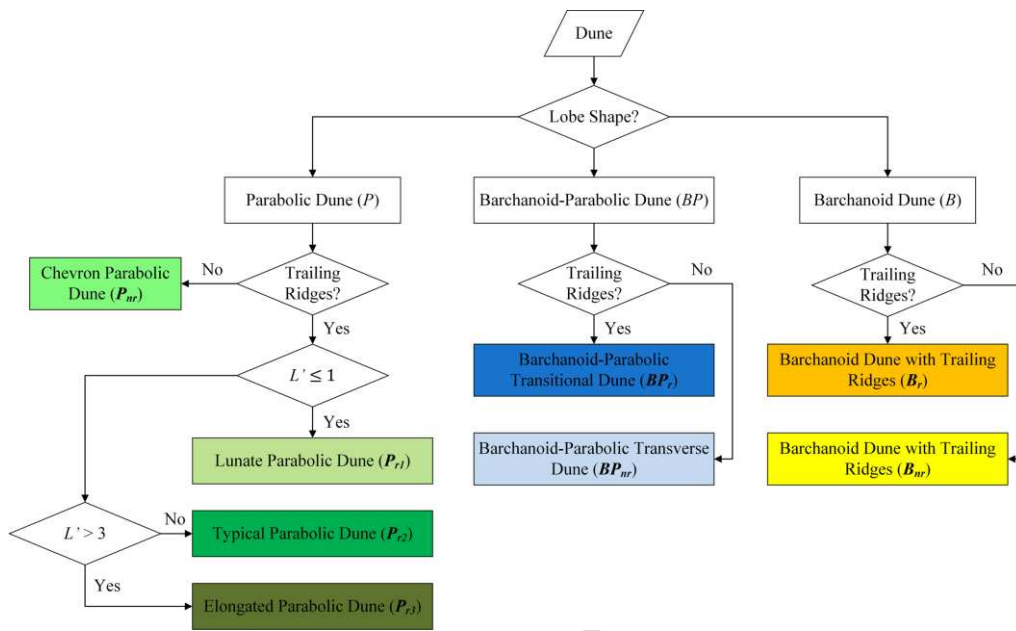
(a)
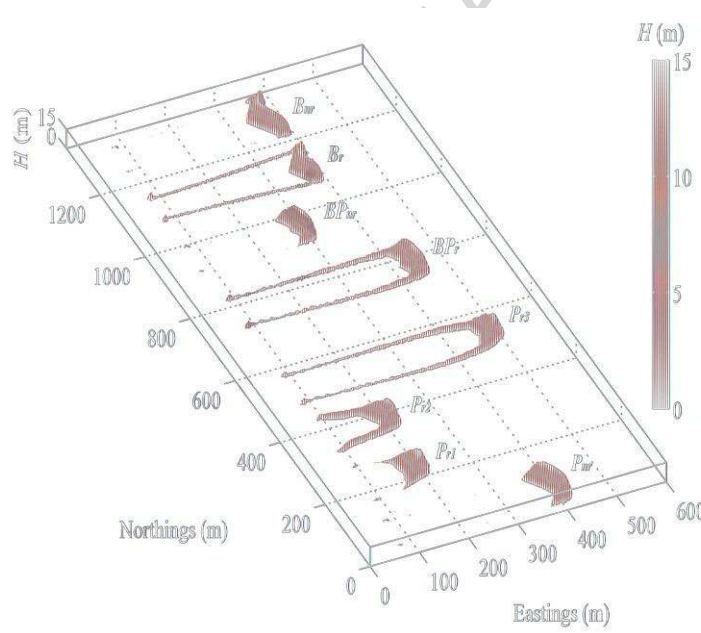
(b)

Figure 7. The classification of eight resulting dune types: (a) decision flow diagram for identification; and (b) visual examples (note that the vertical scale is exaggerated).

(a)   (b)
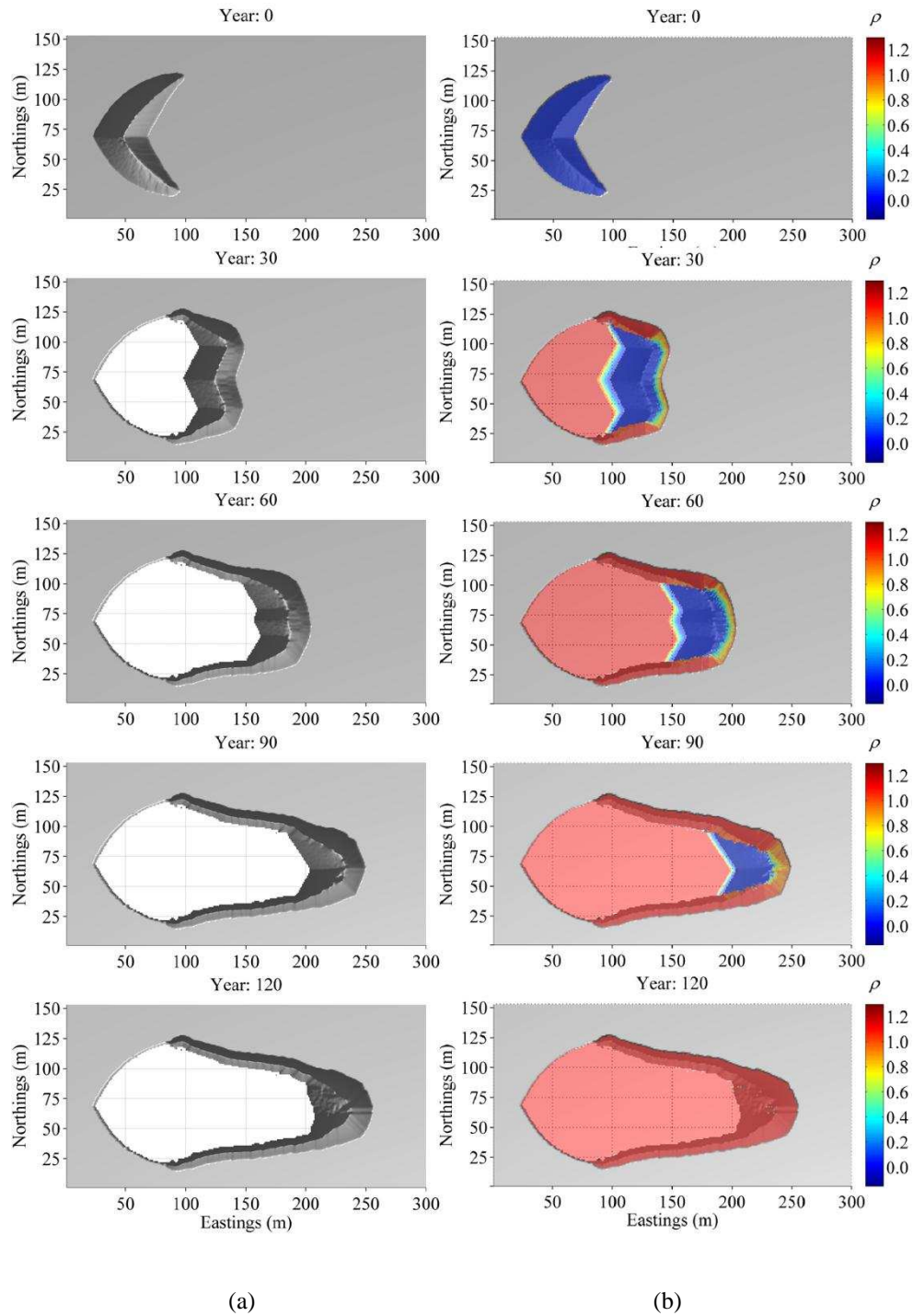
Figure 8. Example of a simulated barchan-to-parabolic dune transformation; q = 20 m^3 m^{-1} yr^{-1}, H$_0$ = 9.2 m, D$_0$ = 0.6 m, $\tau_{E\_physioMax}$ = -2.3 m season^{-1}, and $\tau_{D\_physioMax}$ = 3.0 m season^{-1}. (a) Topography shown in shaded 3D (white deflation plain indicating exposed non-erodible base of the modelling domain; see Video F.1. (b) Spatial distribution of vegetation effectiveness. Vegetation on the surrounding plain is masked out, so that stabilised arms and frontal edge of dune can be clearly identified; see Video F.2.

(a)

(b)

(c)
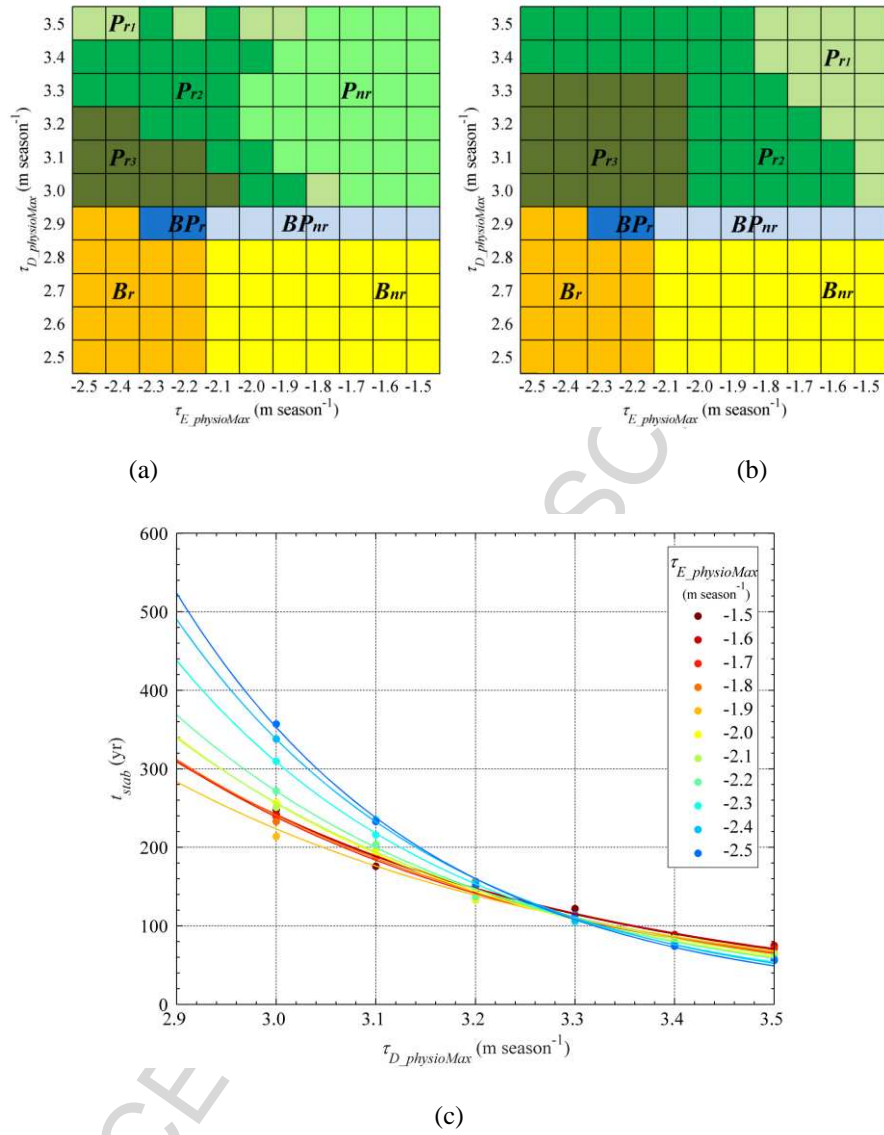
Figure 9. Dune transformations resulting from different combinations of $\tau_{E\_physioMax}$ and $\tau_{D\_physioMax}$; $H_0 = 5.2$ m, $D_0 = 0.6$ m, and $q = 20$ m^3 m^{-1} yr^{-1}. (a) Dune types at t_{tran}, with colour-coding same as Figure 10. (b) Dune types at t_{stab}. (c) t_{stab} as a function of $\tau_{D\_physioMax}$ for the parabolic dune types (upper half of phase diagrams), with colour representing different levels of $\tau_{E\_physioMax}$; curves are fitted exponential functions ($R^2 > 0.97$).
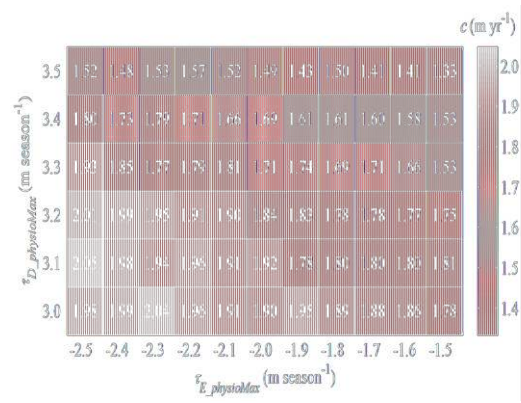
(a)
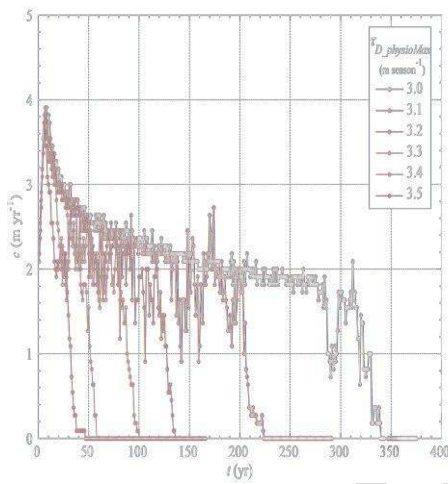
(b)
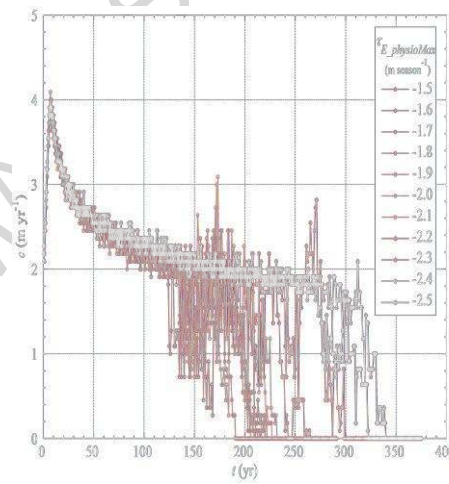
(c)

Figure 10. (a) The average migration rate of resulting parabolic dunes (c) under different $\tau_{E\_physioMax}$ and $\tau_{D\_physioMax}$; $H_0 = 5.2$ m, $D_0 = 0.6$ m, and $q = 20$ m^3 m^{-1} yr^{-1}. (b) Change in c over time under different $\tau_{D\_physioMax}$ (data smoothed with 11-year window); $\tau_{E\_physioMax} = -2.5$ m season^{-1}. (c) change in c over time under different $\tau_{E\_physioMax}$ (data smoothed with 11-year window); $\tau_{D\_physioMax} = 3.0$ m season^{-1}.

(a)   (b)
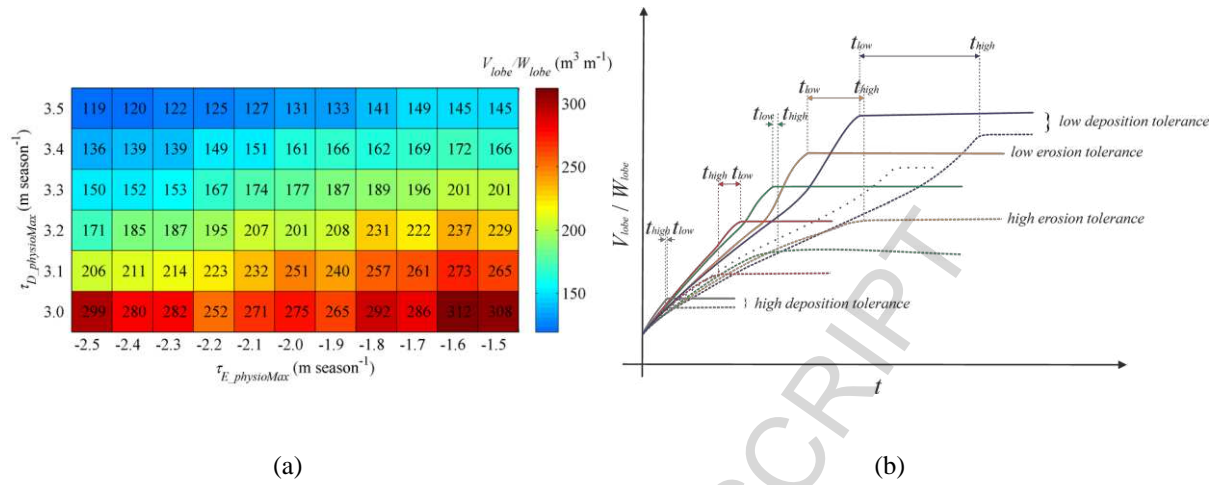
Figure 11. (a) The sand volume of the dune lobe per width at t_{stab}; $H_0 = 5.2$ m, $D_0 = 0.6$ m, and $q = 20$ m^3 m^{-1} yr^{-1}. (b) Schematic overview of V' dynamics during the dune transformation, summarising 66 scenario results. Each colour represents a group of simulations with constant deposition tolerance. Within each group, solid and dashed lines outline upper and lower boundaries representing scenarios with lowest and highest erosion tolerance, respectively. t_{low} and t_{hight} denote t_{stab} at lowest and highest erosion tolerance within each deposition tolerance group, respectively.

(a)

(b)

(c)

(d)
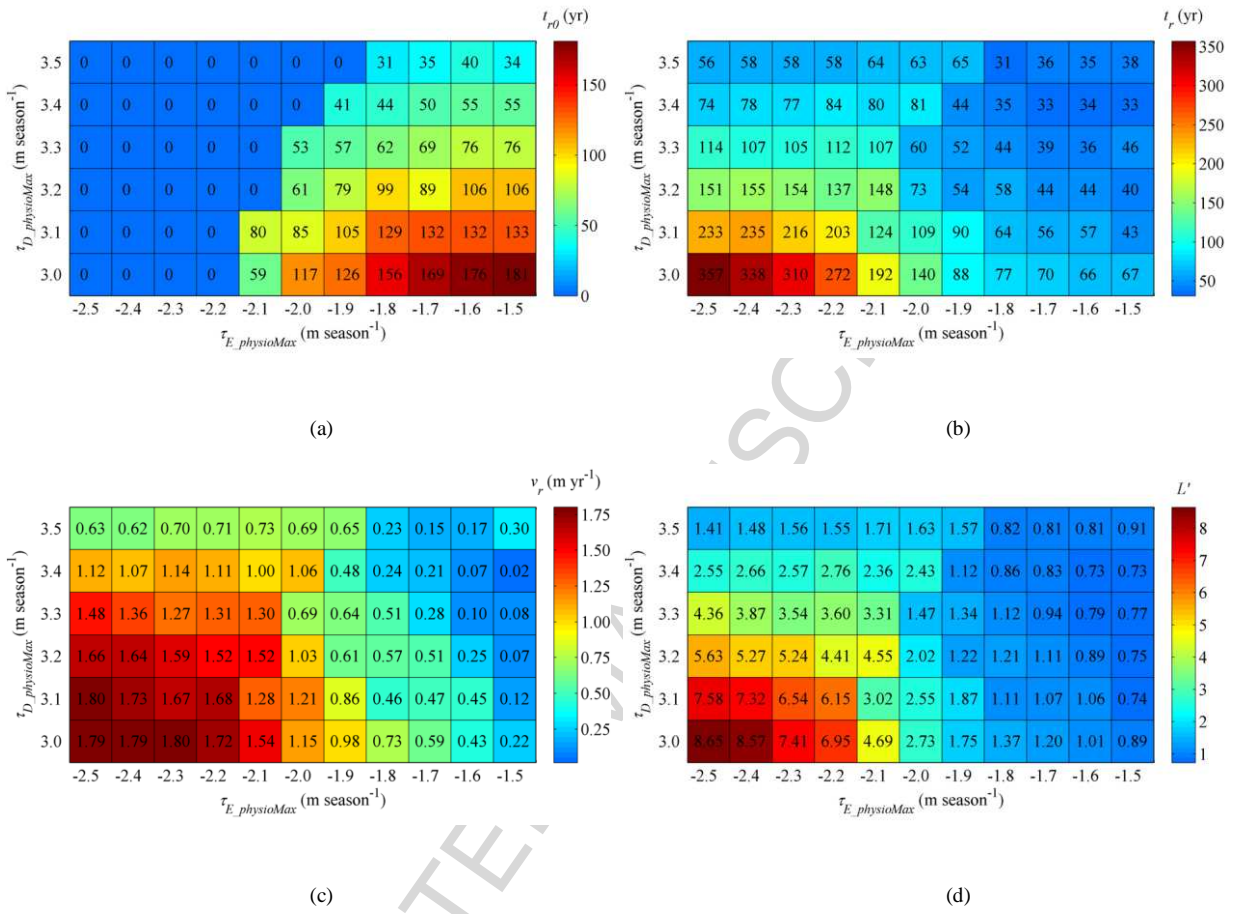
Figure 12. The (a) arms-initiation time (t_{r0}), (b) arms-elongating duration (t_r), (c) arms-elongating rate (v_r), and (d) L' at t_{stab} under different $\tau_{E\_physioMax}$ and $\tau_{D\_physioMax}$. $H_0 = 5.2$ m, $D_0 = 0.6$ m, and $q = 20$ m^3 m^{-1} yr^{-1}.

(a)

(b)   (c)
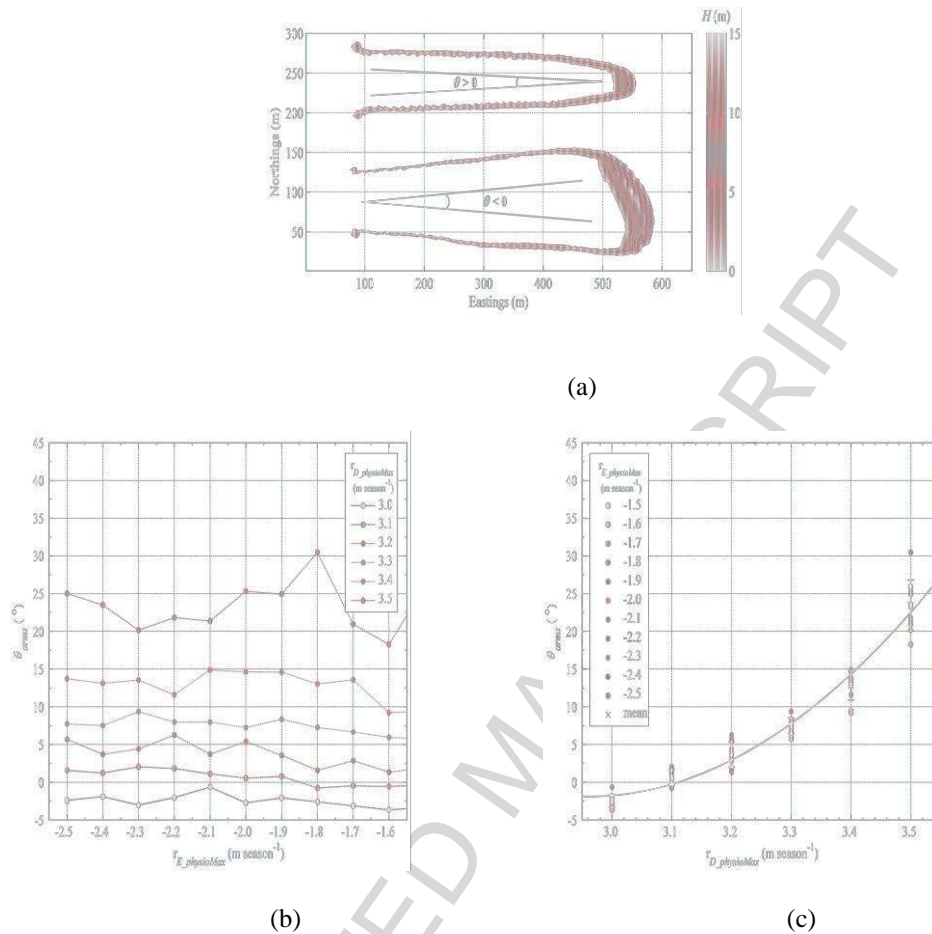
Figure 13. (a) The arms-developing angle, θ_{arms}, of parabolic dunes. A linear regression line is fitted through the crest

of each arm (Appendix D) in plan view, and the angle θ between the two regression lines is obtained. (b) and (c)

show θ_{arms} at t_{stab} under different erosion and deposition tolerances. Cross and whiskers in (c) denote mean $\pm$ standard

deviation of θ_{arms} from different erosion tolerances at a given deposition tolerance, and the black line is the best-fitted

2nd order polynomial regression curve through the means ($R^2 = 0.99$). $H_0 = 5.2$ m, $D_0 = 0.6$ m, and $q = 20$ m^3 m^{-1} yr^{-1}.

(a)   (b)
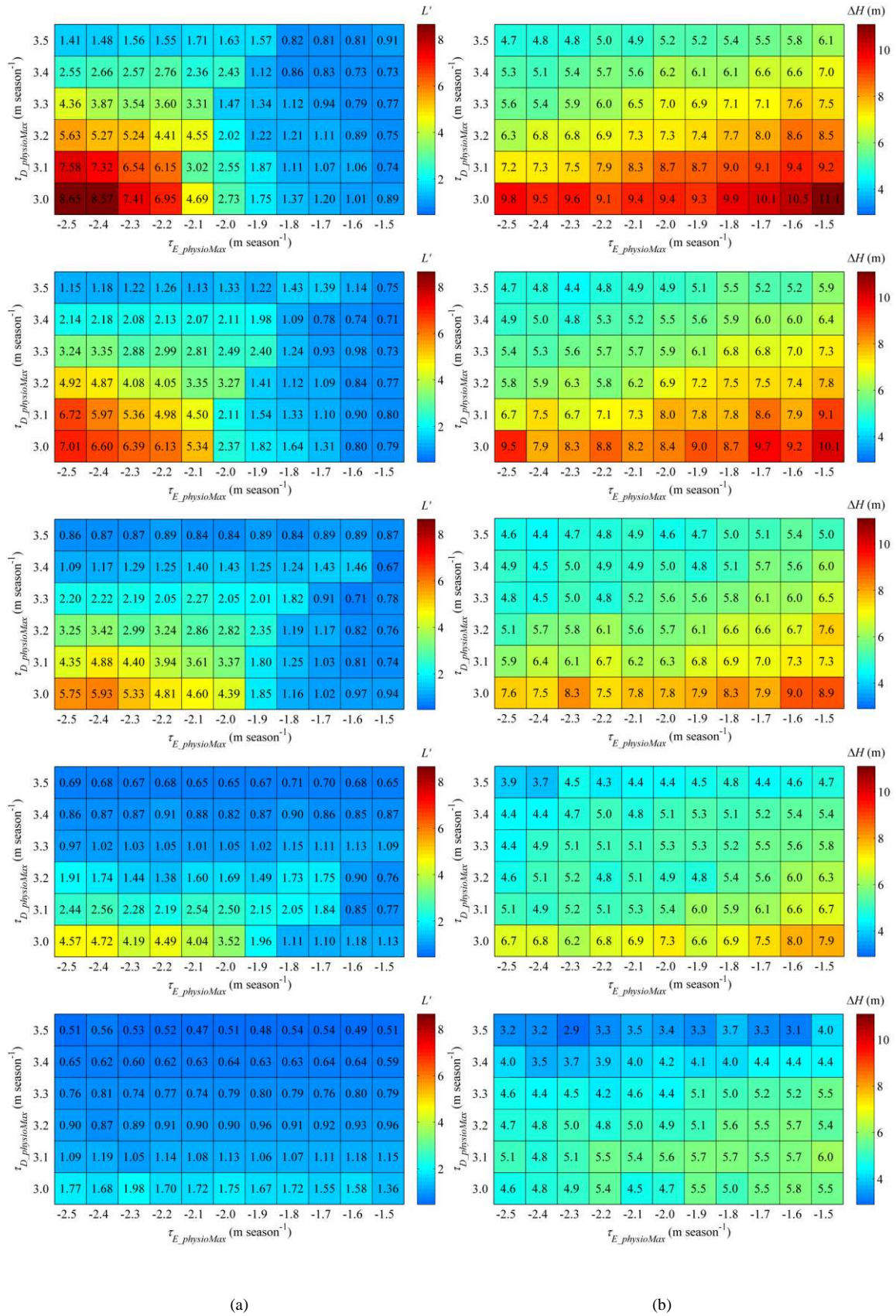
Figure 14. (a) L' and (b) the increase in dune height relative to H_0 (ΔH) of resulting parabolic dunes at t_{stab}. H_0 increases from 5.2 m to 9.2 m.

38

(a) $\tau_{D\_physioMax}$ = 3.0 m season^{-1}

(b) $\tau_{D\_physioMax}$ = 3.1 m season^{-1}

(c) $\tau_{D\_physioMax}$ = 3.2 m season^{-1}
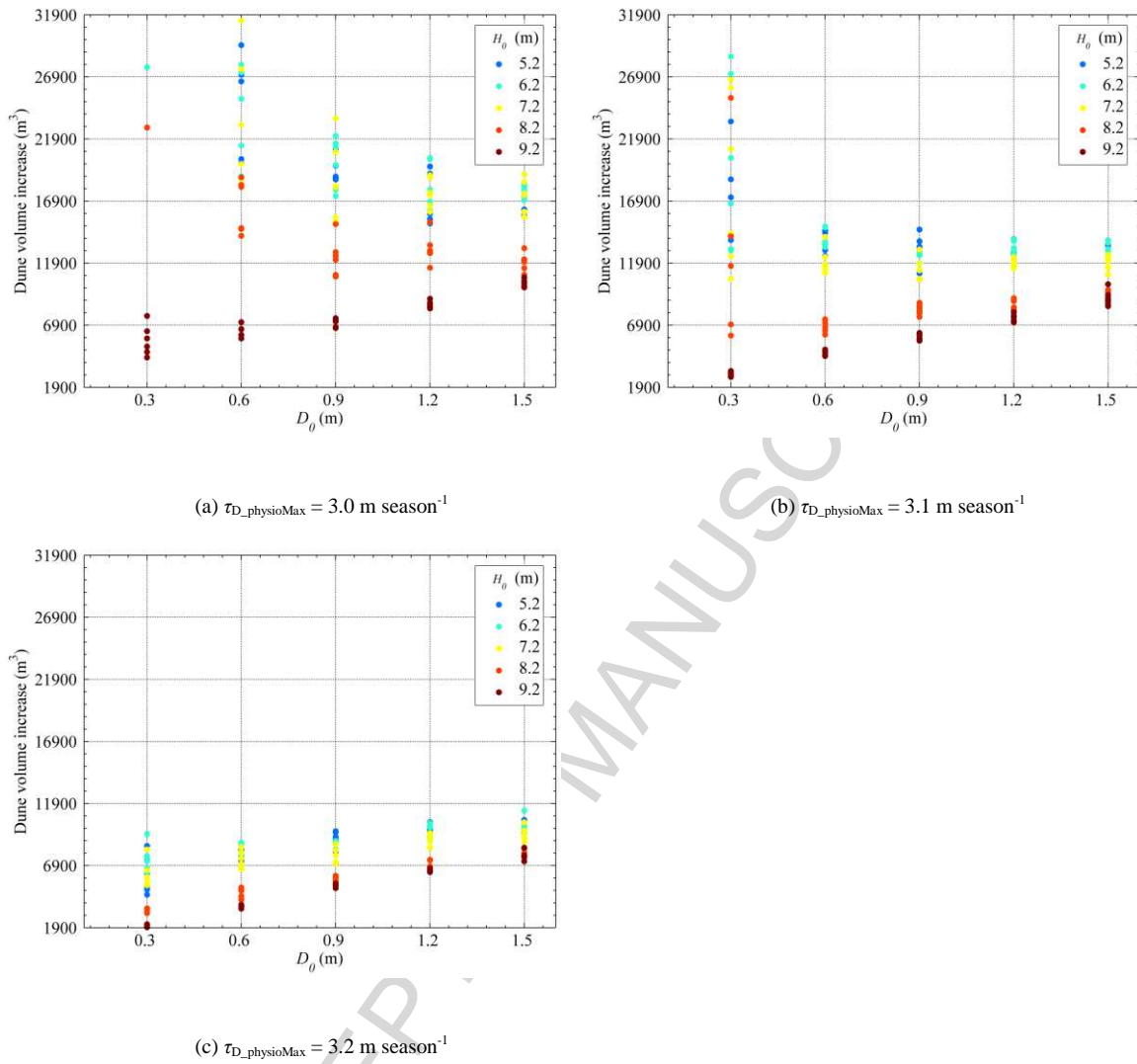
Figure 15. Dune volume increase relative to the initial barchan at t_{stab}. Multiple dots of the same colour denote simulations under different erosion tolerances, from -2.0 to -2.5 m season^{-1} with 0.1 m season^{-1} steps. When a deposition tolerance is 3.0 m season^{-1}, as D_0 increases, sand gained from the substratum also increases for a large H_0 of 9.2 m, but decreases for smaller ones. However, when a deposition tolerance increases to 3.2 m season^{-1}, a thicker substratum leads to a slight increase in the sand volume of the resulting parabolic dunes regardless of H_0. A relatively large deposition tolerance significantly limits small initial barchans gaining sand from a relatively thin substratum.

(a)

(b)

(c)

(d)
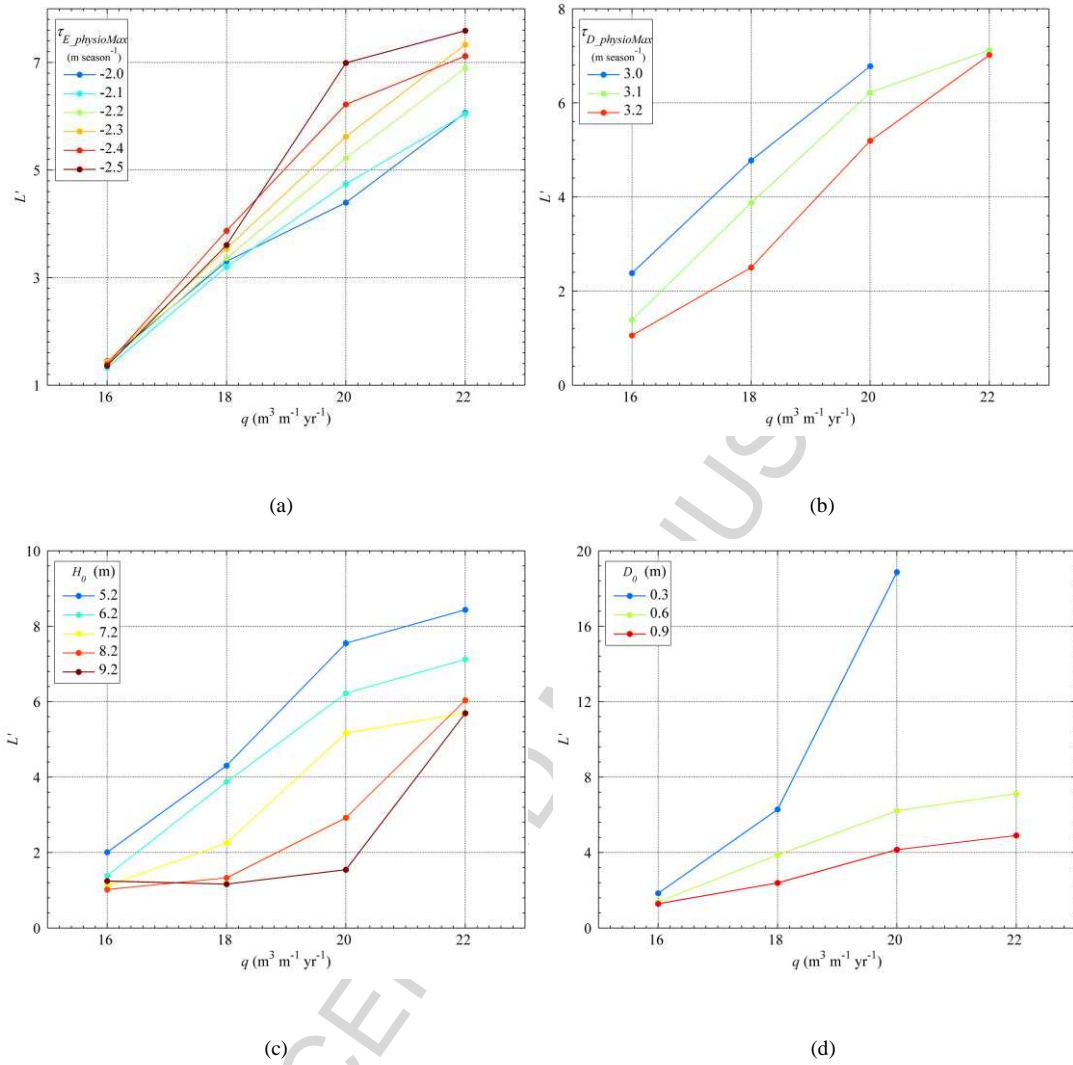
Figure 16. Relationship between q and L'. (a) H_0 = 6.2 m, D_0 = 0.6 m, and $\tau_{D\_physioMax}$ = 3.1 m season[-1]. (b) H_0 = 6.2 m, D_0 = 0.6 m, and $\tau_{E\_physioMax}$ = -2.4 m season[-1]. (c) D_0 = 0.6 m, $\tau_{D\_physioMax}$ = 3.1 m season[-1], and $\tau_{E\_physioMax}$ = -2.4 m season[-1]. (d) H_0 = 6.2 m, $\tau_{D\_physioMax}$ = 3.1 m season[-1], and $\tau_{E\_physioMax}$ = -2.4 m season[-1]. An increase in q generally promotes the development of more elongated parabolic dunes. A higher erosion tolerance increases L' significantly when q is relatively large, but exerts a minimal impact when q decreases to 16 m[3] m^{-1} yr. In contrast, the impact of the deposition tolerance is relatively uniform regardless of the magnitude of q. A smaller H_0 is more sensitive to a change in q. There is no substantial increase in L' for a larger barchan ($H_0 \geq$ 8.2 m) until q increases up to 20 m[3] m^{-1} yr^{-1}. The q plays a more considerable role at a thinner substratum; in particular, a great surge occurs at the D_0 of 0.3 m.

(a)

(b)

(c)

(d)
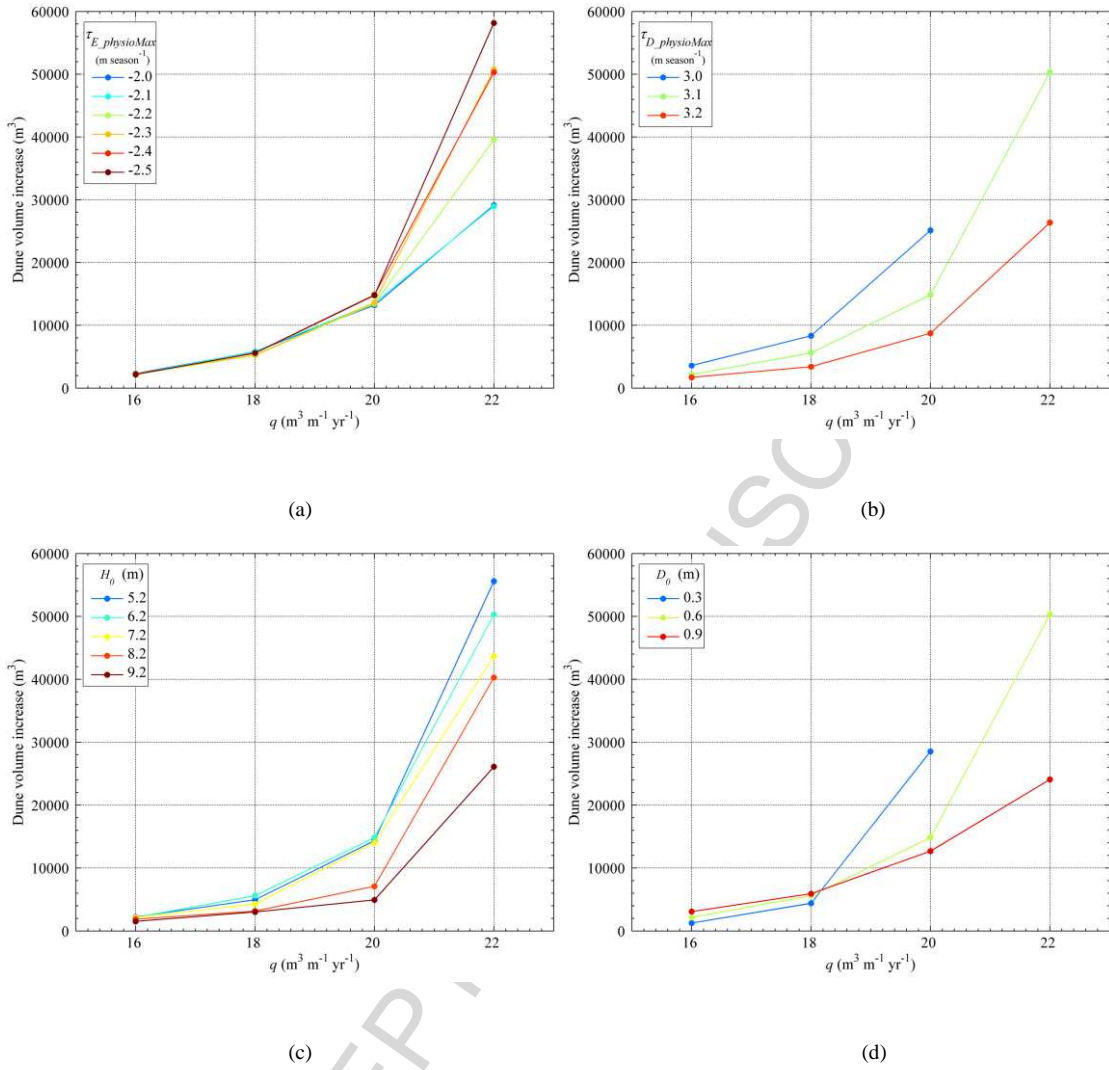
Figure 17. Relationship between q and dune volume increase. (a) H_0 = 6.2 m, D_0 = 0.6 m, and $\tau_{D\_physioMax}$ = 3.1 m season^{-1}. (b) H_0 = 6.2 m, D_0 = 0.6 m, and $\tau_{E\_physioMax}$ = -2.4 m season^{-1}. (c) D_0 = 0.6 m, $\tau_{D\_physioMax}$ = 3.1 m season^{-1}, and $\tau_{E\_physioMax}$ = -2.4 m season^{-1}. (d) H_0 = 6.2 m, $\tau_{D\_physioMax}$ = 3.1 m season^{-1}, and $\tau_{E\_physioMax}$ = -2.4 m season^{-1}.

41

(a)

(b)
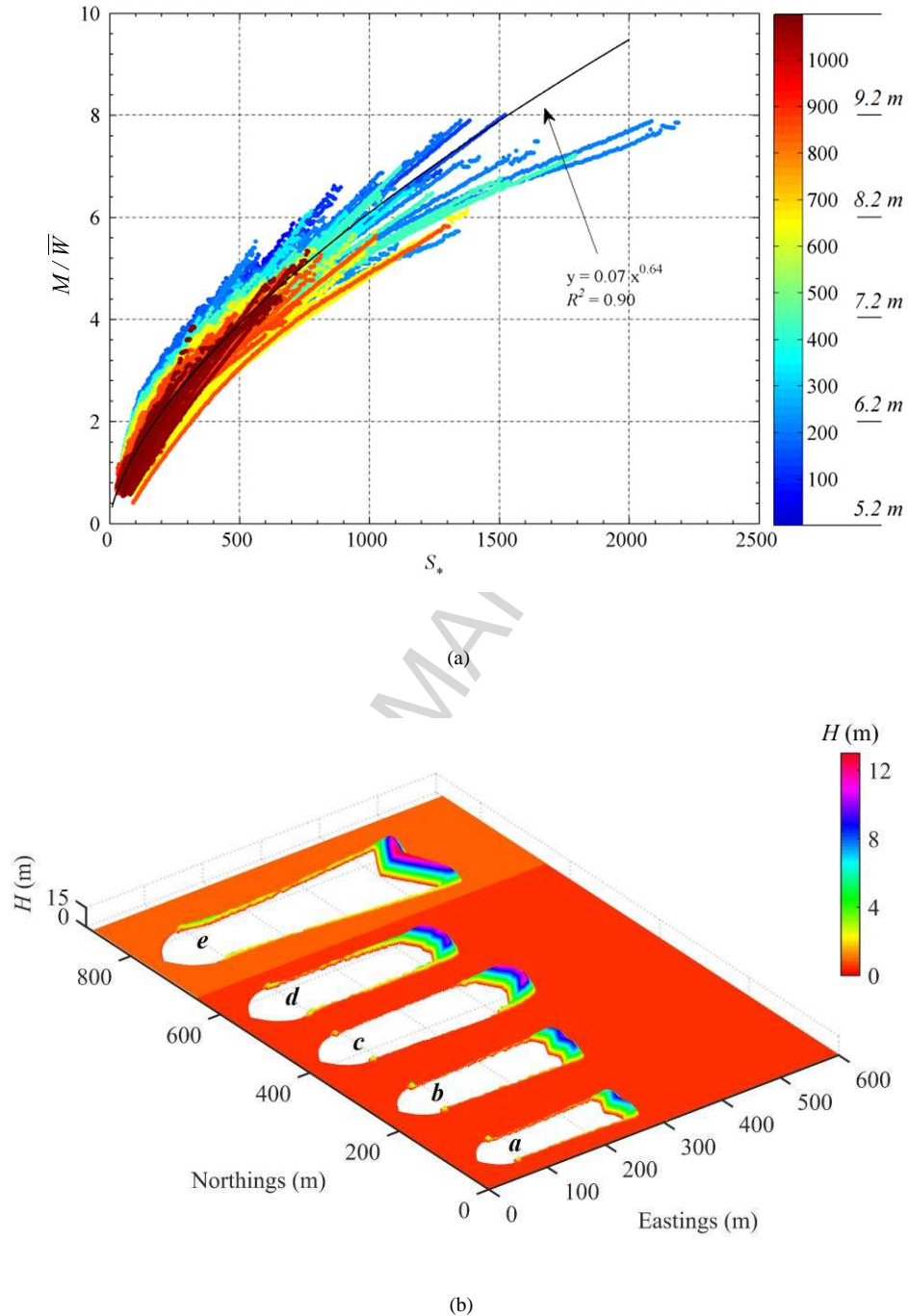
Figure 18. (a) Relation between S_* and $M/\overline{W}$. Simulations are ordered by H_0 first, then q, and D_0. The Jet Stream colour scheme is used in which colour changes gradually from dark blue to dark red; blue, cyan, yellow, orange, and red are roughly in accordance with simulations starting from a barchan at 5.2 m, 6.2 m, 7.2 m, 8.2 m, and 9.2 m respectively, although each simulation is in effect represented by a different colour according to its ordered relative position on the list. The black line shows the best-fit curve by using 1097 simulations and 80241 points (1-year steps), excluding simulations with a substratum thickness of 0.3 m because of a great magnitude of randomness (see text in detail). (b) DEMs of dunes with the same S_* of 400.

42
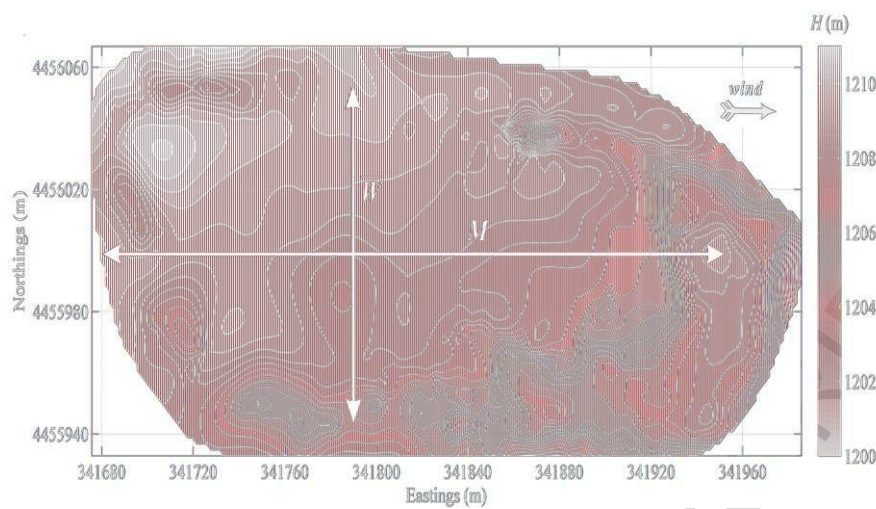
(a)
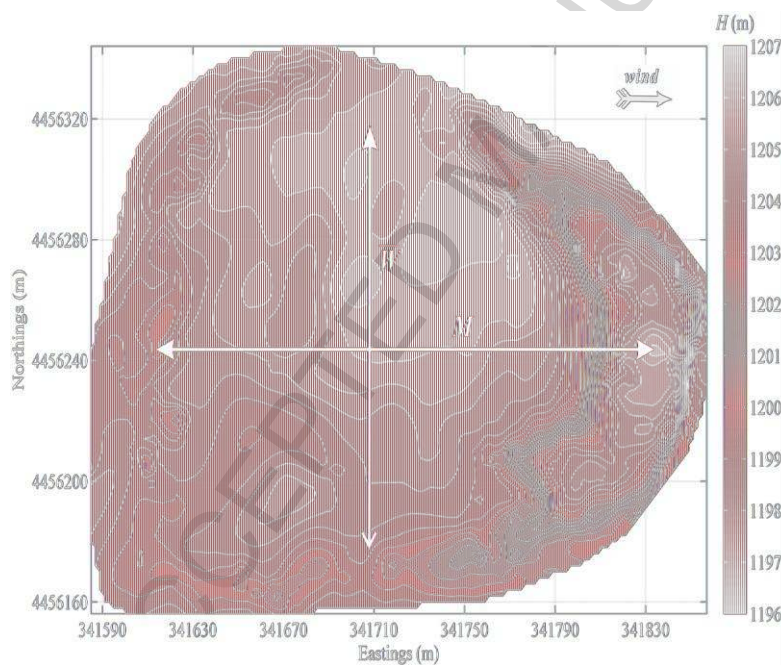
(b)

Figure 19. DEMs of parabolic dunes (a) D1 and (b) D2 in 2012. Contour lines are in 0.4 m steps.

<div align="center">(a)</div>

<div align="center">(b)</div>
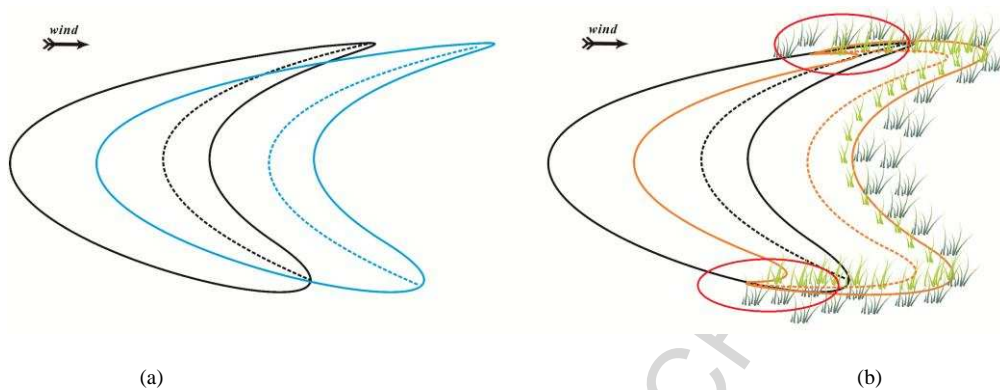
Figure 20. Comparison of a barchan dune migration on a bare surface (a) and on a vegetated surface (b). The initial barchan is outlined in black, and the dunes outlined in blue and orange denote dune morphology at a different time. Red circles indicate the initiation of trailing-ridges caused by sand-trapping of vegetation.

(a)   (b)

(c)   (d)
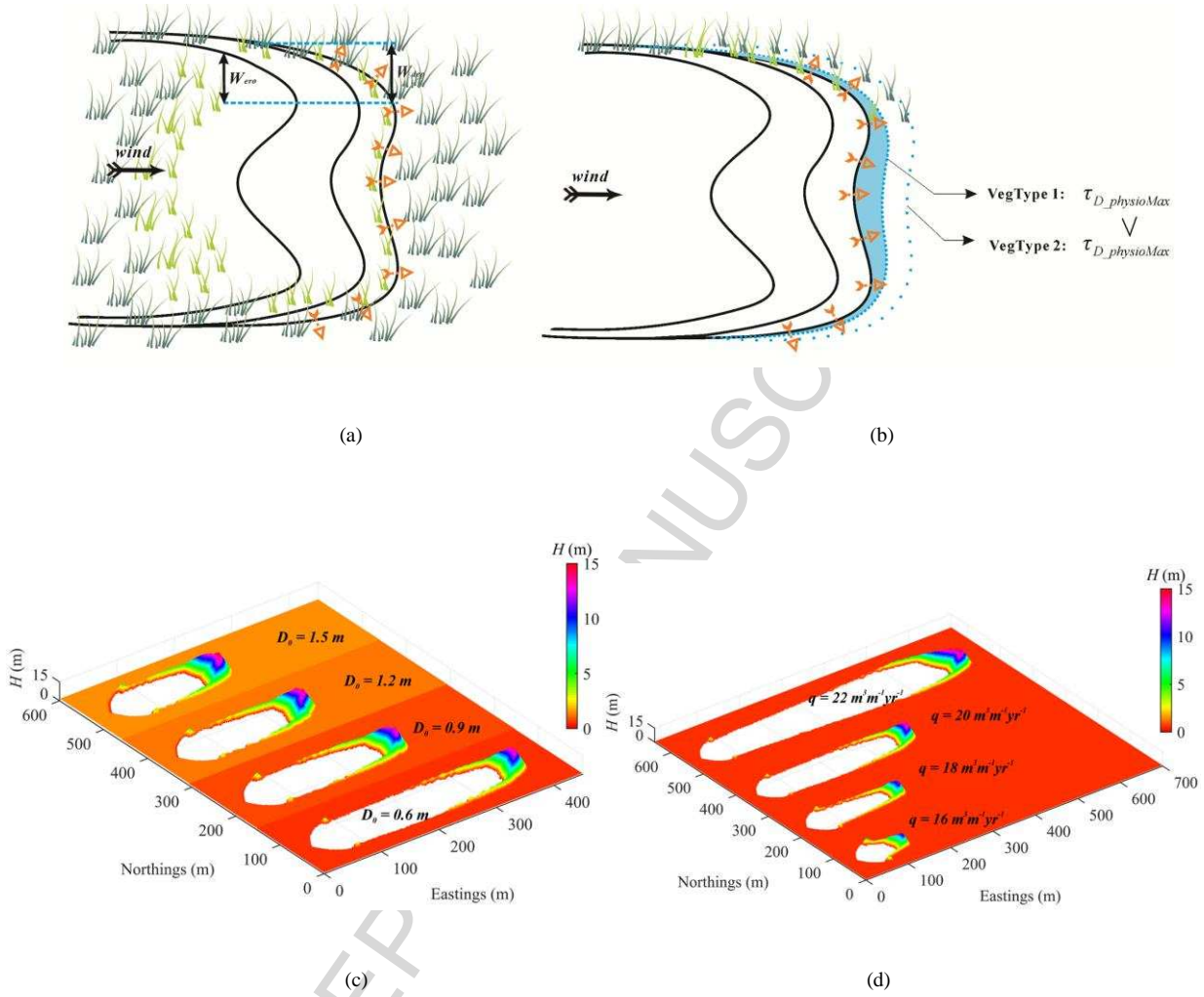
Figure 21. (a) Schematic illustration of slow-down effect of lobe edges due to sand avalanching on the deposition slope. W_{ero} and W_{dep} are effective erosion width (the width of a lobe section perpendicular to winds on the windward slope) and the associated deposition width (the associated width of the lobe section for deposition of sand from the W_{ero}) respectively. Orange arrows denote sand avalanching directions on the lee slopes. (b) Schematic illustration of how the vegetation deposition tolerance determines the arms-developing angle. (c) Influence of D_0 on arms-developing angle. $q = 20$ m^3 m^{-1} yr^{-1}, $H_0 = 6.2$ m, $\tau_{E\_physioMax} = -2.0$ m season^{-1}, and $\tau_{D\_physioMax} = 3.1$ m season^{-1}. D_0 increases from 0.6, 0.9, 1.2 to 1.5 m in sequence, resulting in an arms-developing angle of 3˚, 6˚, 7˚ and 8˚ respectively. (d) Influence of q on arms-developing angle. $D_0 = 0.6$ m, $H_0 = 6.2$ m, $\tau_{E\_physioMax} = -2.0$ m season^{-1}, and $\tau_{D\_physioMax} = 3.1$ m season^{-1}. q increases from 16, 18, 20 to 22 m^3 m^{-1} yr^{-1} in sequence, resulting in an arms-developing angle of 38˚, 11˚, 3˚, and - 4˚ respectively.
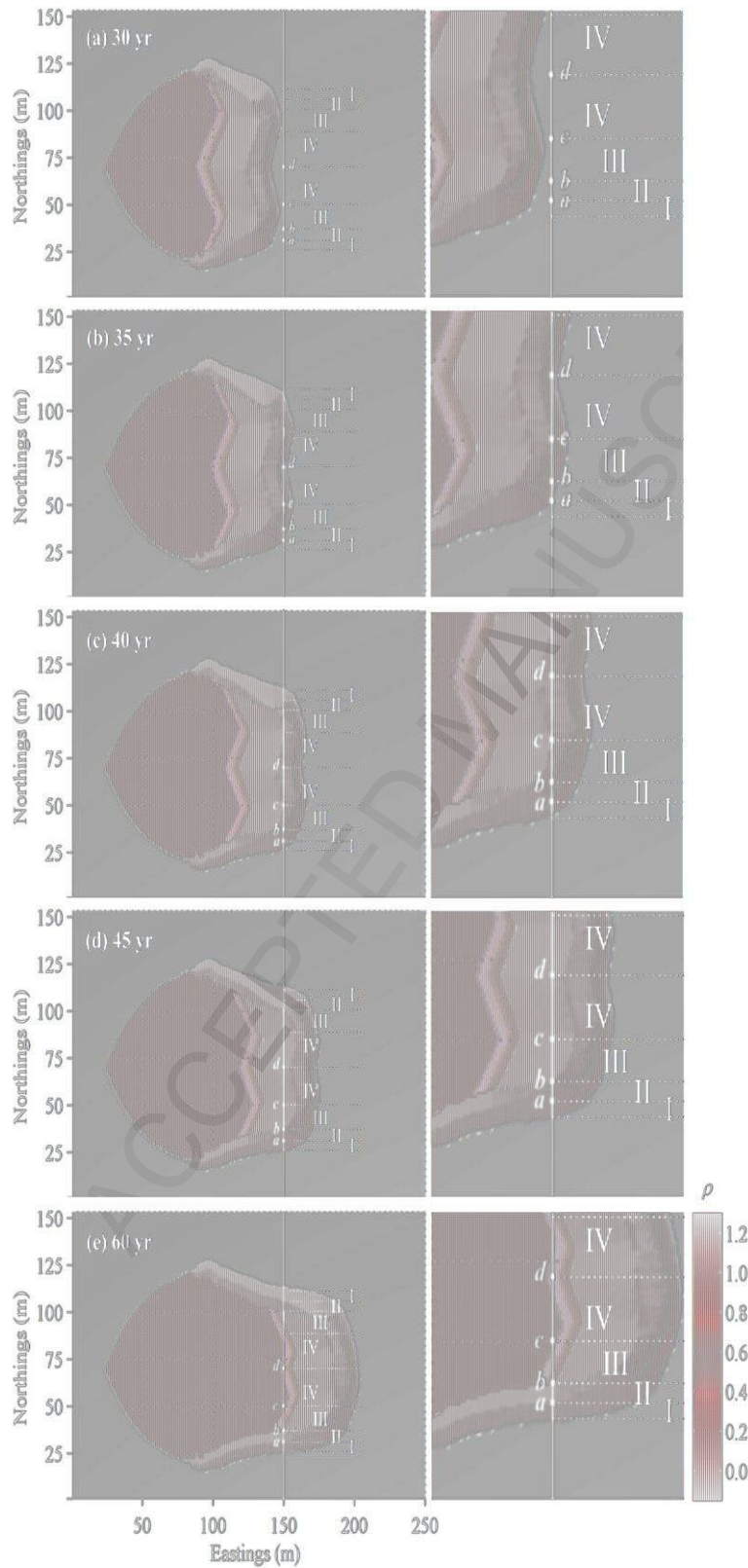
Figure 22. The eco-geomorphic interaction and the barchan-to-parabolic dune transformation. $q = 20$ m^3 m^{-1} yr, H$_0$ = 9.2 m, D$_0$ = 0.6 m, $\tau_{E\_physioMax}$ = -2.3 m season^{-1}, $\tau_{D\_physioMax}$ = 3.0 m season^{-1}. The a (150, 31), b (150, 37), c (150, 50), and d (150, 70) reflect boundaries between different eco-geomorphic interaction zones (I, II, III, and IV). See Video F.3.

46

(a) Zone I: 25 m-a

(b) Zone II: a-b

(c) Zone III: b-c

(d) Zone IV: c-d
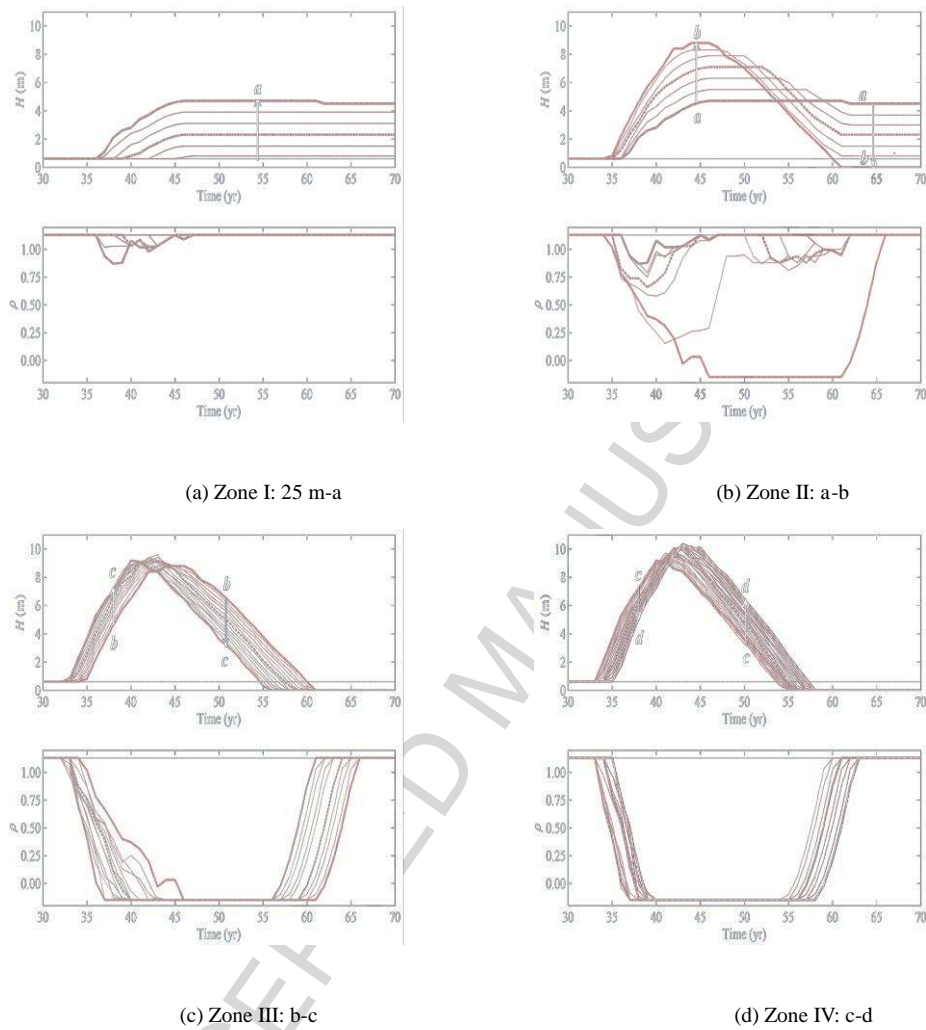
Figure 23. Topography and vegetation change over time in different eco-geomorphic interaction zones. $q = 20$ m^3 m^{-1} yr, $H_0 = 9.2$ m, $D_0 = 0.6$ m, $\tau_{E\_physioMax} = -2.3$ m season^{-1}, $\tau_{D\_physioMax} = 3.0$ m season^{-1}. The a, b, c, and d are boundaries of different eco-geomorphic interaction zones across the transverse section at 150 m of eastings shown in snapshots in Figure 22. Each line/colour represents a 1 by 1 m^2 cell along the transverse section. The arrow shows the location of cells from south to north.

47
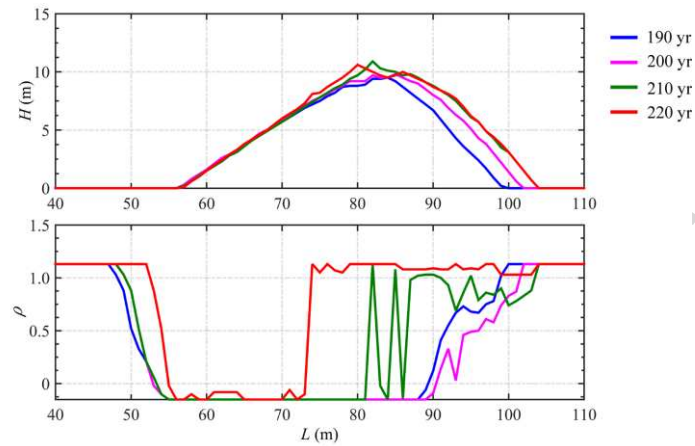
(a)
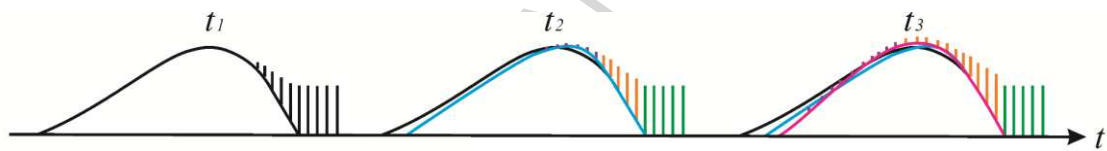
(b)

Figure 24. (a) An example of a dune transect (upper panel) and vegetation change (lower panel) over time. $H_0 = 5.2$ m, $D_0 = 0.6$ m, $\tau_{E\_physioMax} = -2.0$ m season^{-1}, and $\tau_{D\_physioMax} = 3.0$ m season^{-1}. To facilitate comparison, dune profiles at different times all start from the same horizontal location. From 190 yr to 200 yr, the dune transect keeps migrating and the highest vertical position on the lee slope where vegetation can grow remains similar; then, after 210 yr, it stops migrating and sand accumulates on the upper slope of the lee side, whilst vegetation encroaches further up to the crest. Vegetation subsequently extends to the windward side at 220 yr and eventually stabilises the whole dune transect. (b) The interrelationship between the dune profile and the vegetation growth when sand transport is insufficient to eliminate vegetation on the lee slope. Blank bars represent vegetation on the migrating dune transect; green bars represent vegetation at steady maximum; orange bars represent vegetation experiencing growth; and magenta bars represent new vegetation.

48

Table 1. Dimensions of five initial barchans.

Barchan	H (m)	W (m)	L (m)	Sand volume (m^3)
a	5.2	72	45	3448
b	6.2	80	53	5241
c	7.2	86	59	7528
d	8.2	94	66	10359
e	9.2	100	73	13780

Table 2. Sand transport regime in the study region.

Season	p_e	p_d	p_{dn}	l (m)	RDP (%)	Iterations
Apr-Jun	1	0.6	0.4	1	30	35
Jul-Sep	1	0.6	0.4	1	12	15
Oct-Dec	1	0.6	0.4	1	25	30
Jan-Mar	1	0.6	0.4	1	33	40
Sum					100	120

Table 3. Representative simulations at their specified stabilising times with the same S_* of 400.

Dune #	H_0 (m)	D_0 (m)	$\tau_{E\_physioMax}$ (m season^{-1})	$\tau_{D\_physioMax}$ (m season^{-1})	q (m^3 m^{-1} yr^{-1})	t (yr)	M (m)	$\overline{W}$ (m)	$M/\overline{W}$
a	5.2	0.6	-2.4	3.0	20	78	223	67	3.33
b	6.2	0.6	-2.3	3.2	22	94	263	79	3.33
c	7.2	0.6	-1.8	3.0	20	144	314	91	3.45
d	8.2	0.6	-2.2	3.2	22	130	294	87	3.38
e	9.2	0.9	-2.4	3.1	22	188	376	113	3.33

Table 4. Calculation of initiation times of barchan-to-parabolic dune transformations in the field.

Dune #	H_0 (m)	D_0 (m)	$\tau_{E\_physioMax}$ (m season^{-1})	$\tau_{D\_physioMax}$ (m season^{-1})	q (m^3 m^{-1} yr^{-1})	M (m)	$\overline{W}$ (m)	t (yr)
D1	4	0.6	-2.0	3.0	20	270	110	**46.7**
D2	8	0.6	-2.0	3.0	20	220	140	**46.5**